UNIVERSITEIT VAN PRETORIA
UNIVERSITY OF PRETORIA
YUNIBESITHI YA PRETORIA

Optoelectronic characterisation of AlGaN based Schottky Barrier Diodes

by

Phuti Ngako Mahloka Ngoepe

Submitted in partial fulfilment of the requirements for the degree

MAGISTER SCIENTIAE

in the Department of Physics

in the Faculty of Natural and Agricultural Science

University of Pretoria

PRETORIA

February 2013

Supervisor: Prof. W.E. Meyer

Co-supervisor: Dr. M. Diale

© University of Pretoria

I, **Phuti Ngako Mahloka Ngoepe**, declare that the thesis/dissertation, which I hereby submit for the degree Magister Scientiae at the University of Pretoria, is my own work and has not previously been submitted by me for a degree at this or any other tertiary institution.

SIGNATURE: ..…………………………...

DATE: ……………………………………....

ACKNOWLEDGEMENTS

I would like to express my sincere appreciation to the following people and institution:

- The Divine Father who has given me a reality to live within and a purpose to live for.
- My supervisor Prof. Walter Meyer for the faith and support that he has shown in me.
- My co-supervisor Dr. Mmantsae Diale for encouragement to complete this project.
- Prof. Danie Auret for being an inspiration to me by his hard work.
- Prof. Johan Malherbe for his help throughout my physics studies.
- Prof. Chris Theron for his leadership as the head of the physics department.
- Mrs. Laeticia Cilliers for her kind heart and appreciating the tutoring work that I do.
- Dr. Matthias Schmidt for his enthusiasm and his insightful input in my life and work.
- My colleagues Dr. Wilbert Mtangi, Mmusi Gopane, Jimmy Mokoena, Louwrens van Schalkwyk, Hannes de Meyer, Matshisa Legodi, Johan Janse van Rensburg, Sergio Coelho, Alex Paradzah, Helga Danga, Fred-Joe Nambala, Dr. Jackie Nel and Dr. Claudia Zander amongst others in the physics department who have given me the support and help to finish this work.
- Prof. Albert Chawanda for his guidance and willingness to help where necessary.
- The National Research Foundation for financial support.
- My parents, Tlabo and Mapula, for the never ending faith, support, guidance and love.
- My beloved siblings Amo, Noko, and Magashe for being there for me.
- My late grandfather Noko Ngoepe for inspiring our family and showing us the importance of education.
- My uncle Prof. Phuti Ngoepe for inspiring me to do physics.
- My extended family who have been supporting, inspiring, motivating, and praying for me to finish.
- The many friends that I have made throughout my life.

UNIVERSITEIT VAN PRETORIA
UNIVERSITY OF PRETORIA
YUNIBESITHI YA PRETORIA

Optoelectronic characterisation of AlGaN based Schottky Barrier Diodes

by

Phuti Ngako Mahloka Ngoepe

Submitted in partial fulfilment of the requirement for the degree MAGISTER SCIENTIAE in the Faculty of Natural and Agricultural Science, Department of Physics, University of Pretoria.

Supervisor: Prof. W. E. Meyer

Co-supervisor: Dr. M. Diale

SUMMARY

Recent advances in growth techniques have lead to the production of high quality GaN and this has played a vital role in the improvement of GaN based devices. A number of device types can be produced from GaN. Spectrally selective devices can be produced by creating ternary or quaternary material systems by partially substituting either Al or In for Ga in GaN. This allows a wide spectral range that can be achieved ranging from the visible to the ultraviolet. The applications of detectors based on these material systems are vast and include areas such as biological, military, environmental, industrial and scientific spheres.

In front illuminated Schottky barrier photodetectors, two major factors influencing the sensitivity of the device are the reverse leakage current and the transparency of the Schottky contact. In order to reduce the reverse current of semiconductor based devices, increase the barrier height, and enhance the adhesion of a metal on a semiconductor it is important to subject the contact to annealing. Annealing studies have been performed on AlGaN based photodiodes to investigate the evolution of the optical and electrical properties.

In this study, the electrical and optical characteristics of AlGaN based Ni/Au and Ni/Ir/Au Schottky photodiodes were investigated. The electrical properties of the photodiodes were

optimised by annealing in an Ar ambient. An increase in the Schottky barrier height and a decrease in the reverse leakage current were observed with increasing annealing temperature up to 500 ^{o}C. This effect was observed for both the Ni/Au and Ni/Ir/Au photodiodes.

The optical characteristics of the photodiodes, which include the responsivity and the quantum efficiency, were also investigated. UV/visible rejection ratios of as high as 10^3 were obtained. The transmittance of Ni/Au and Ni/Ir/Au metal layers deposited on a quartz substrate were optimised by annealing. This was under the same ambient conditions as the Schottky photodiode. The transmittance increased with annealing temperature for the Ni/Au metal layer whereas it decreased at higher temperatures for the Ni/Ir/Au layer. The transmittance of the Ni/Au metal layer reached as high as 85 % after 500 ^{o}C annealing. The transmittance of the Ni/Ir/Au only reached a high of 41 % after 400 ^{o}C annealing.

TABLE OF CONTENTS

1 INTRODUCTION 1
REFERENCES 4
2 THEORETICAL BACKGROUND 5
2.1 INTRODUCTION 5
2.2 SEMICONDUTOR 5
2.2.1 Crystal structure 5
2.2.2 Optical properties 7
2.2.3 Crystal growth 9
2.3 METAL-SEMICONDUCTOR CONTACTS 10
2.3.1 Energy bands 10
2.3.2 Image force lowering 15
2.3.3 Current transport mechanisms 17
2.3.3.1 Thermionic emission 18
2.3.3.2 Quantum mechanical tunneling 21
2.3.3.3 Generation recombination 22
2.3.4 Electrical characterisation of Schottky barrier diode 23
2.3.4.1 Introduction 23
2.3.4.2 Current-voltage 25
2.3.4.3 Capacitance-voltage 27
2.3.5 Ohmic contact 29
2.3.6 Photonic devices 30
2.3.6.1 Photodetectors 31
2.3.6.2 Photodiodes 31
2.3.6.3 Schottky photodiode 32
REFERENCES 35
3 EXPERIMENTAL TECHNIQUES 37
3.1 INTRODUCTION 37
3.2 SAMPLE PREPARATION 37
3.3 DEPOSITION 38
3.3.1 Electron beam system 39
3.3.2 Resistive evaporator system 39

3.4 ANNEALING 40
3.5 MEASUREMENT TECHNIQUES 41
3.5.1 Electrical characterisation 41
3.5.2 Optical characterisation 42
3.5.2.1 Photocurrent measurements 42
3.5.2.2 Transmission measurements 44
REFERENCES 45
4 RESULTS AND DISCUSSION 1 46
4.1 INTRODUCTION 46
4.2 EXPERIMENTAL 46
4.3 RESULTS AND DISCUSSION 46
4.4 CONCLUSION 52
REFERENCES 53
PUBLICATION 54
5 RESULTS AND DISCUSSION 2 57
5.1 INTRODUCTION 57
5.2 EXPERIMENTAL 57
5.3 RESULTS AND DISCUSSION 58
5.3.1 Electronic properties 58
5.3.2 Responsivity 61
5.3.3 Current voltage measurements under different illumination wavelengths 62
5.3.4 Transmission 65
5.4 CONCLUSION 66
REFERENCES 67
6 CONCLUSIONS 68

CHAPTER 1

INTRODUCTION

The development of ultraviolet detection research started gaining momentum when the ultraviolet segment of the electromagnetic spectrum began receiving attention. Specifically, the so called “solar blind” region of the UV spectrum is technologically important, as the atmosphere completely filters out this portion of the UV spectrum coming from the sun. This opens a field of research on the various applications for very sensitive short range detection of UV radiation in broad daylight. These include detection of corona discharges in power lines, fire detection systems and missile plume detection. These applications have lead to the development of filters, detectors, light sources and other related devices [1]. Ultraviolet detectors generally fall into two categories namely photodetectors and thermal detectors. In photodetectors an electrical signal is generated directly due to the absorption of radiation. These kinds of detectors tend to be highly spectrally selective. Thermal detectors depend on the thermo-electric properties of a material being heated by the incident radiation [2]. In this study photodetectors were investigated.

There are a number of materials which have been identified as important semiconductors for photon detector fabrication. These include SiC, GaN, Si, GaAs, GaP and diamond. The III-V nitrides are top contenders for photon detection materials due to the fact that they have good thermal conductivity, chemical inertness, and high thermal stability [1]. This means that photodetectors made from III-V nitrides can be operated under harsh conditions and still maintain their functionality.

Solar blind ultraviolet applications require detectors that respond to ultraviolet radiation, but not to sunlight. Traditionally, filters have been used to block visible light. Another approach is to use the fact that semiconductors, in the ideal case, do not absorb photons with an energy lower than their bandgap. Therefore, detectors made on wide bandgap semiconductors can be made spectrally selective, so that they do not respond to radiation with a wavelength longer than their cutoff wavelength. Wide bandgap photodetectors are preferred over other semiconductor based photodiodes such as Si due to the fact that they do not require bulky,

inefficient and expensive filters to block the visible range of the sun. Also, these photodetectors are highly spectrally selective.

There has been a keen interest in aluminium gallium nitride ($Al_xGa_{1-x}N$) as a UV detector material since, including the above characteristics of III-V nitrides, it is a wide bandgap semiconductor. Its bandgap can be varied between 3.4 eV and 6.2 eV. This variation in the bandgap corresponds to a spectral range of 365 to 200 nm and is achieved by varying the aluminium fraction, x. The spectral range can be extended by introducing InN to form a quaternary alloy namely indium aluminium gallium nitride ($In_xAl_yGa_{1-x-y}N$). InN has a bandgap of 1.9 eV which corresponds to a wavelength of 653 nm [3]. This means that InAlGaN based devices can have a range from the ultraviolet right up to the visible spectrum. Lee *et al.* fabricated a photodetector demonstrating the use of the InAlGaN material system [4].

There are a number of applications which photodetectors can be used for. These include space-to-space communication, solar UV radiation monitoring, chemical sensing, flame detection, and missile plume detection [5]. A solar blind detector is especially required for the last three applications. A solar blind detector by definition is a detector which is insensitive to wavelengths that are greater than 285 nm. Due to absorption in the earth's atmosphere, there are few photons from the sun which are less than 285 nm which are able to reach the earth, therefore these detectors do not respond to sunlight [2].

In order to improve the electrical properties of photodiodes, the reverse leakage current has to be decreased and the Schottky barrier height increased. One method of doing this is subjecting the photodiode to annealing. Kim *et al.* used it as a method for passivating the metal/AlGaN interface [6]. Annealing studies have been done by Miura *et al.* using different metal systems. They investigated these metals for the fabrication of high electron mobility transistors [7]. Chang *et al.* carried out annealing analysis of metal-semiconductor-metal (MSM) photodetectors [8].

The objective of this study is to add to the knowledge about the evolution of the electrical and optical properties of AlGaN based Schottky photodiodes with annealing. This included investigating both the Ni/Au and Ni/Ir/Au metal systems. In choosing AlGaN, we aimed to produce a photodetector which has a high spectral selectivity, low noise, and high quantum efficiency. These are characteristics of a good photodetector.

Chapter 2 gives the theoretical background of the semiconductor and the types of characterisation techniques of the metal-semiconductor contact. Section 2.1 is an introduction to the chapter and section 2.2 explains the crystal structure, optical properties and the growth technique of the semiconductor. Section 2.3 describes the properties of the metal-semiconductor contact. These include both the optical and electrical properties.

In chapter 3, the experimental techniques are explained. Section 3.1 consists of a brief introduction to the chapter. Section 3.2 gives the details of the sample preparation, while section 3.3 explains how the electron beam and resistive evaporation systems were employed to deposit metals on the AlGaN wafers. Section 3.4 is about the procedures used for annealing the samples. Section 3.5 concludes the chapter by describing the characterisation techniques used. Both electrical and optical techniques are described.

Chapter 4 presents the evolution of the electrical and optical characteristics with thermal annealing of a Ni (50 Å)/ (50 Å) Au Schottky photodiode. Chapter 5 gives a comparison of the electrical and optical characteristics measured for Ni (20 Å)/ Au (50 Å) and Ni (20 Å)/ Ir (30 Å)/ Au (50 Å) Schottky photodiodes after annealing at different temperatures. Chapter 6 gives a summary and conclusion of the obtained results.

REFERENCES

[1] M. Razeghi, and A. Rogalski, J. Appl. Phys. **79** (10), (1996) 7433.

[2] M. Razeghi, Proc. of the IEEE **90,** (2002) 1006.

[3] S.N. Mohammad and H. Morkoc, Prog. Quant. Electr. **20** (5/6), (1996) 361.

[4] H.C. Lee, Y.K. Su, J.C. Lin, Y.C. Cheng, T.C. Li, and K.J. Chang, Solid State Electron. **54**, (2010) 488.

[5] O. Ambacher, J.Phys. D: Appl. Phys. **31**, (1998) 2653.

[6] H. Kim, M. Schuette, H Jung, J. Song, J. Lee, and W. Lu, Appl. Phys. Lett. **89**, (2006) 053516.

[7] N. Miura, T. Nanjo, M. Suita, T. Oishi, Y. Abe, T. Ozeki, H. Ishikawa, T. Egawa, and T. Jimbo, Solid State Electron. **48**, (2004) 689.

[8] P.C. Chang, C.H. Chen, S.J. Chang, Y.K. Su, C.L. Yu, P.C. Chen and C.H. Wang, Semicond. Sci. Technol. **19**, (2004) 1354.

CHAPTER 2

THEORETICAL BACKGROUND

2.1 INTRODUCTION

In this chapter the theory relating to the study of materials used and devices fabricated is explained. Section 2.2 looks at the semiconductor used in the study. The properties of aluminium gallium nitride ($Al_xGa_{1-x}N$) are discussed. These include the structural and optical properties. The growth of the material is also discussed. In section 2.3 the metal semiconductor contact is discussed. The energy bands, transport mechanism and electrical properties resulting from the formation of such contacts are described. At the very end of the chapter the properties of a Schottky photodiode are discussed.

2.2 SEMICONDUTOR

2.2.1 Crystal structure

Aluminium gallium nitride (often also written as $Al_xGa_{1-x}N$) is a ternary semiconductor that is formed by substituting a proportion of Ga atoms in gallium nitride (GaN) with Al. This makes it a useful semiconductor for fabricating devices such as UV detectors, lasers and LEDs as its bandgap can be varied from 3.44 to 6.2 eV [1]. It can be seen as being formed from two binary compounds namely aluminium nitride (AlN) and GaN. These are group III nitrides that crystallize in either the hexagonal wurtzite or the cubic zincblende crystal structure [2]. The material used in this study has a wurtzite crystal structure as shown in Fig.1. According to Vegard's law the lattice parameters of GaN and AlN will change linearly with increasing Al content. The distances between the Ga-N and Al-N bonds vary slightly thus implying that the variations in bond lengths between ions in AlGaN are probably preserved by bond angle distortions [3].

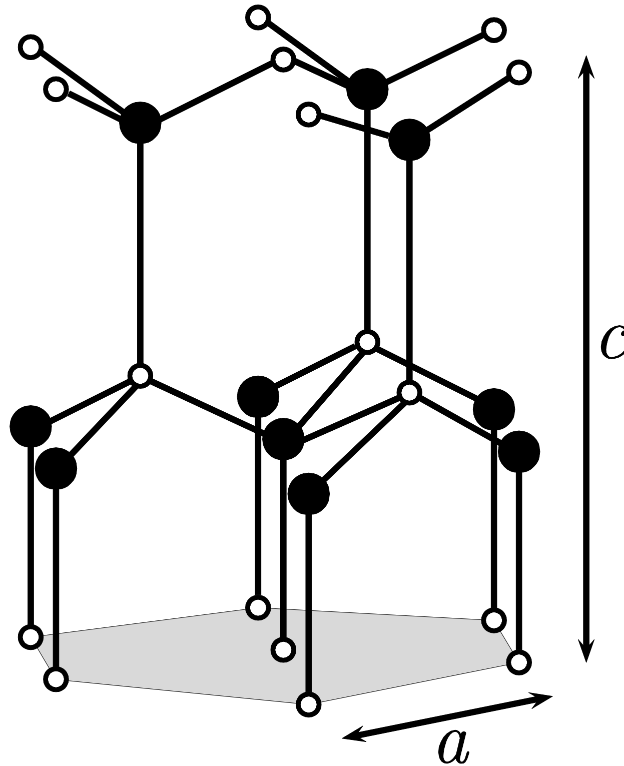

Fig. 1 The hexagonal wurzite structure of AlGaN (dark spheres = Gallium/ Aluminium, light spheres = Nitrogen) [4].

AlGaN is a direct bandgap semiconductor and its optical bandgap is dependent on the composition of the Al as shown in Fig. 2. The relationship between AlN and GaN ratios and bandgap is written in the form:

$$Eg_{AlGaN}(x) = Eg_{GaN}{}^{*}(1-x) + Eg_{AlN}{}^{*}x - b^{*}x^{*}(1-x) \tag{2.1}$$

where E_g is the optical bandgap, x the AlN molar fraction and b the bowing factor. The bowing factor is a parameter that shows the extent of the nonlinearity of the relationship between the energy bandgap and the molar fraction. The bowing can either be upwards or downwards depending on the system characteristics. When b is positive there is upward bowing and when it is negative, downward bowing [5]. Indium nitride (InN) is a binary compound can be combined with GaN to form indium gallium nitride (InGaN). This increases the range with which GaN based devices can operate as InN has a bandgap energy of 1.9 eV. Various other properties of AlN and GaN are written in Table 1 below.

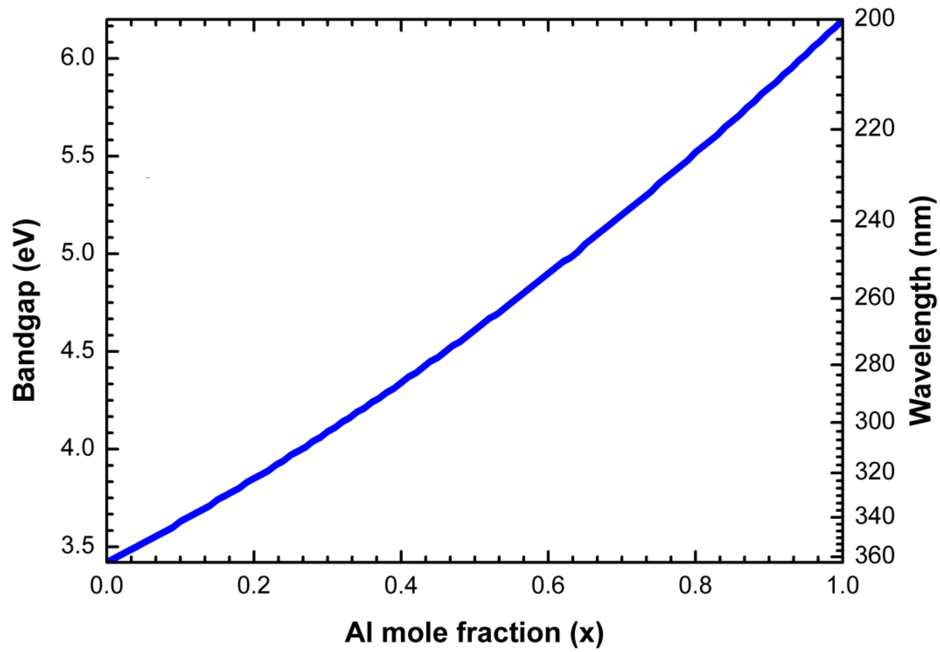

Fig. 2 The variation of the wavelength of incident radiation and bandgap of Al_xGa_xN with Al composition [6].

Table 1 Properties of AlN and GaN [7].

	Aluminium nitride (AlN)	Gallium nitride (GaN)
Electron effective mass, m_e	0.48	0.20
Melting point (^{o}C)	3000	> 1700
Lattice constant, *a* (Å)	3.11	3.189
Lattice constant, *c* (Å)	4.98	5.185
Static averaged dielectric constant	8.5	8.9
Bandgap @ 300 K (eV)	6.2	3.39

2.2.2 Optical properties

A photon that is incident on the surface of a solid can either be reflected by or penetrate through the surface of the material. The photon can be absorbed depending on the absorption

coefficient of the material. Photons with energies less than the bandgap are transmitted while those with energies greater than the bandgap are absorbed. The absorbed photons create electron hole pairs and the photo-generated carriers contribute to the conductivity of the semiconductor [8].

The energy of the radiation can be related to the material that is absorbing the radiation near its surface by the absorption coefficient using the following equation:

$$\alpha \sim (h\nu - E_g)^{\gamma} \tag{2.2}$$

where $h\nu$ is the photon energy and γ is a value which depends on the type of optical transition from the valence band to the conduction band. The value of γ can be 1/2 and 3/2 for allowed direct and forbidden direct transitions respectively. For indirect transitions the value is 2. All the above are for a one electron approximation. For an exciton state the value of γ is 1/2 [9]. Fig. 3 shows the difference between the optical transitions which an electron can undergo. These include the direct and indirect transitions.

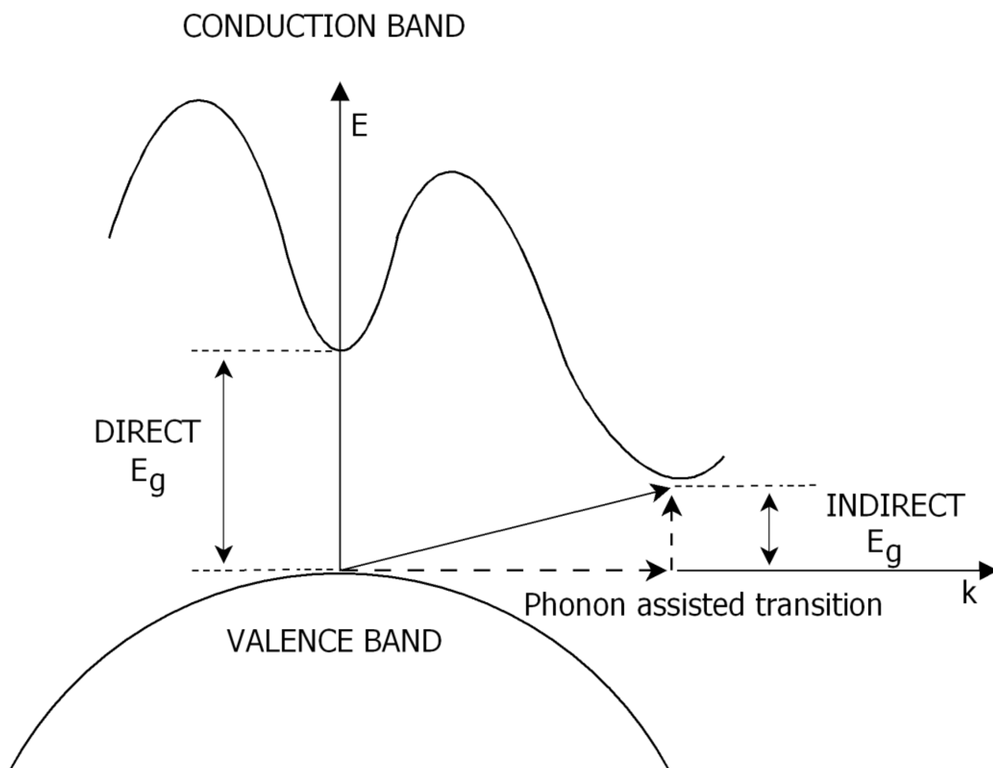

Fig. 3 Optical (bandgap) transitions: direct and indirect transitions [10].

2.2.3 Crystal growth

It is technologically challenging to grow a bulk AlGaN wafer that can be used for device fabrication. This has led to AlGaN based semiconductors being grown using different layers on various substrates such as silicon carbide (SiC) or sapphire (Al_2O_3). The near surface material is then modified to be suitable for semiconductor device fabrication. Deposition techniques such as thermal evaporation, chemical vapour deposition and sputtering have been utilised to produce semiconductors. The structural, physical and chemical properties can have a great impact on device performance [11]. Epitaxial growth is a processing technique that has gained interest as it can be used to grow thin films. The term epitaxy as explained by Tyagi, is used to refer to those processes which are used to grow a crystalline layer of a semiconductor on a crystalline substrate in such a way that the layer grown has the same lattice structure as the substrate [12].

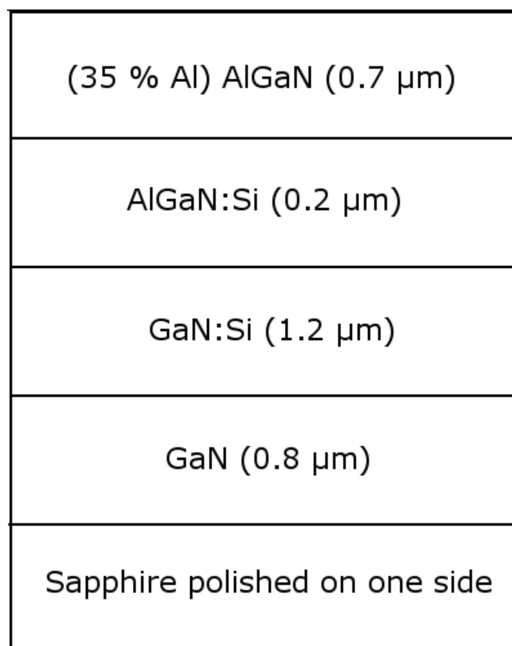

Fig. 4 The different layers of the $Al_{0.35}Ga_{0.65}N$ wafer that was used in this project (not drawn to scale).

In growing thin films on a substrate, the thin film will tend to take the structure of the substrate on which it is grown. In the case where the composition of the thin film is the same as that of the substrate, the deposition is said to be homoepitaxially grown. The growth of two compositionally dissimilar materials is referred to as heteroepitaxial growth. There are a

number of growth techniques that have been used for epitaxial layer deposition. They include the physical deposition such as molecular beam epitaxy (MBE), liquid phase epitaxy (LPE) and the chemical vapour deposition (CVD). Examples of the CVD include hydride vapour phase epitaxy (HVPE) and metal-organic vapour phase epitaxy (MOVPE).

In this study the material that has been used is heteroepitaxially grown AlGaN using HVPE sourced from Technologies and Devices Inc (TDI). The AlGaN was grown in a temperature controlled quartz furnace. Flowing hydrogen chloride (HCl) gas reacts with liquid gallium and/or alluminium. This produces gallium chloride (GaCl) and/or alluminium chloride (AlCl) which then reacts with ammonium gas to form either GaN, AlN or AlGaN [13]. This process can be written in equation form in the following manner:

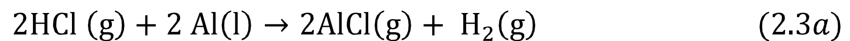

$$2\mathrm{HCl}\ (\mathrm{g}) + 2\ \mathrm{Al}(\mathrm{l}) \rightarrow 2\mathrm{AlCl}(\mathrm{g}) + \mathrm{H}_2(\mathrm{g}) \qquad (2.3a)$$

and/or

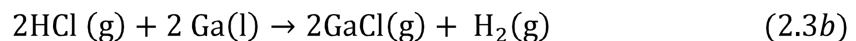

$$2\mathrm{HCl}\ (\mathrm{g}) + 2\ \mathrm{Ga}(\mathrm{l}) \rightarrow 2\mathrm{GaCl}(\mathrm{g}) + \mathrm{H}_2(\mathrm{g}) \qquad (2.3b)$$

Then

$$\mathrm{AlCl}\ (\mathrm{l}) + \mathrm{NH}_3(\mathrm{g}) \rightarrow \mathrm{AlN}(\mathrm{s}) + \mathrm{HCl}(\mathrm{g}) + \mathrm{H}_2(\mathrm{g}) \qquad (2.3c)$$

and/or

$$\mathrm{GaCl}\ (\mathrm{l}) + \mathrm{NH}_3(\mathrm{g}) \rightarrow \mathrm{GaN}(\mathrm{s}) + \mathrm{HCl}(\mathrm{g}) + \mathrm{H}_2(\mathrm{g}) \qquad (2.3d)$$

The layers used to fabricate the wafer that was used for this study are shown in Fig. 4. Sapphire was used as the substrate. On top of the substrate a layer of undoped GaN consisting of a thickness of 0.8 μm was grown. Onto this layer a 1.2 μm thick silicon-doped GaN layer was grown. Next in line was the growth of a 35% Al AlGaN layer which was also silicon doped. This layer had a thickness of 0.2 μm. The last layer that was grown was an AlGaN layer containing 35 % Al which was undoped. This top layer has a thickness of 0.7 μm.

2.3 METAL-SEMICONDUCTOR CONTACTS

2.3.1 Energy bands

Energy bands are useful in showing the electronic states that an electron is allowed or forbidden to occupy in a solid. The energy band structure of a crystalline solid is given by the energy-momentum relationship within a crystal lattice. When a metal and a semiconductor

come into intimate contact with each other, the energy of electrons in the vicinity of the interface are affected. This relationship can be described in terms of the energy bands and Fermi levels in both materials. The ideal energy band relationship is now explained and is shown in Fig. 5. Taking the vacuum level as a reference for the energy levels in the two materials, namely the metal and the semiconductor, the work function is defined as the difference between the Fermi energy and the vacuum level. When the metal and semiconductor are brought into contact with each other, electrons from the conduction band of the semiconductor cross the metal-semiconductor junction into the metal. This occurs because the Fermi level in the semiconductor is higher than in the metal. The energy bands of the semiconductor begin to bend downwards because of the electric field due to the charge building up. The charge build up is caused by the migration of electrons. This continues until the Fermi levels of the metal and semiconductor align.

The Fermi level of the semiconductor is lowered relative to that of the metal by a value equal to the difference between the metal work function and the semiconductor work function. This value is called the contact potential. Since electrons are moving from the semiconductor to the metal, a negative charge is developed on the metal side of the contact and this implies that the semiconductor becomes depleted of electrons. As a result of this, a depletion region is formed in the semiconductor. The depletion region is a space-charge region in which there are almost no conduction electrons and there is a positive net charge due to the ionised donors [14]. In the metal, the electrons accumulate very close to the interface.

The processes described above lead to the formation of a barrier, the height of which is defined according to the Schottky- Mott relationship by:

$$q\phi_B = q(\phi_M - \chi) \tag{2.4}$$

where $q\phi_M$ is the metal work function and $q\chi$ the electron affinity of the semiconductor. The electron affinity can be defined as the amount of energy released when an electron is added to the semiconductor, i.e. the difference between the vacuum level and the conduction band. The barrier prevents electrons from moving easily across the heterojunction between the metal and the semiconductor. Under equilibrium conditions, the number of electrons moving from the metal to the semiconductor are balanced by the number of electrons moving from the semiconductor to the metal.

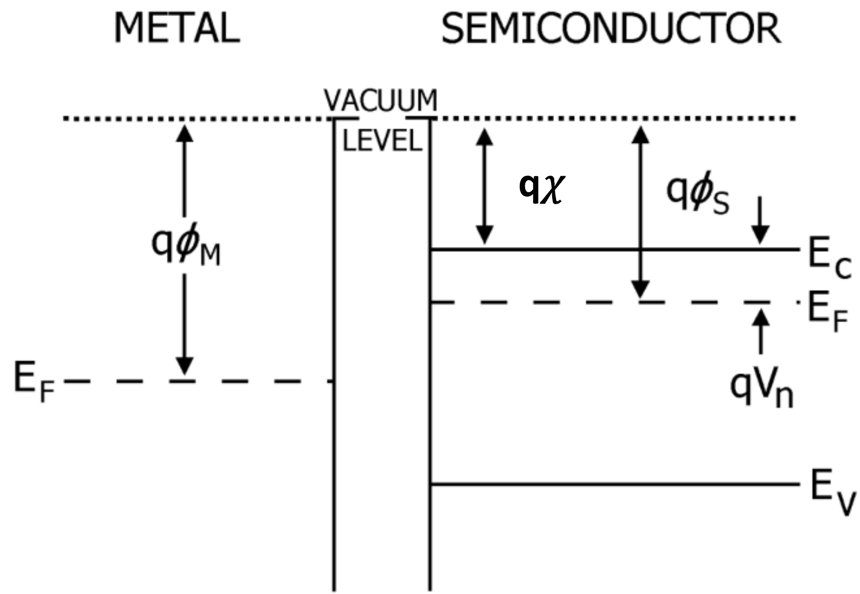

(a)

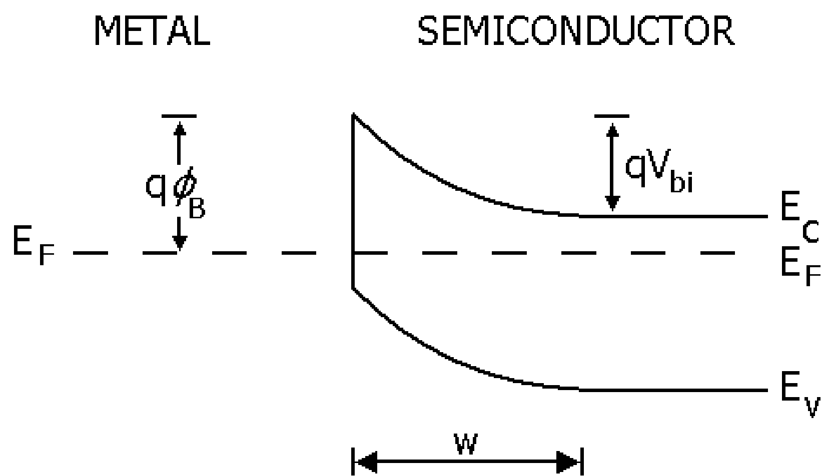

(b)

Fig. 5 Energy band diagrams of a metal and semiconductor (a) Before contact (b) After contact to illustrate the formation of a Schottky barrier [9].

A net flow of electrons can however occur if there is a bias voltage applied. The applied bias can influence how the electrons 'see' the barrier height. There are two bias voltages that can be applied namely the forward and reverse. Under forward bias conditions, a negative potential is applied to the semiconductor, increasing the Fermi level of the semiconductor relative to that of the metal and reducing band bending. The electrons will then 'see' a lower barrier height thus enabling the electrons to move easily across the metal-semiconductor junction, causing a large current to flow.

Under reverse bias conditions, a positive potential is applied and the electrons in the semiconductor 'see' a higher barrier height, reducing the flow of electrons from the semiconductor to the metal. When the bias voltages are applied, the barrier height remains constant for the electrons on the metal side, so a small current of electrons still flows from the semiconductor to the metal. Measuring the current under this condition will yield low current flows across the barrier. Fig. 6 illustrates these phenomena.

The only way that these electrons can overcome the barrier height without an applied bias voltage is if there is radiation that is incident on the metal-semiconductor junction. There are two conditions under which this can happen. The first is when the incident energy of radiation is greater than the barrier height. The second is when incident energy is greater than the bandgap of the semiconductor [10]. The built in voltage V_{bi} is the depth of the conduction band below the barrier height whereas qV_n is the energy difference between the Fermi level and the conduction band.

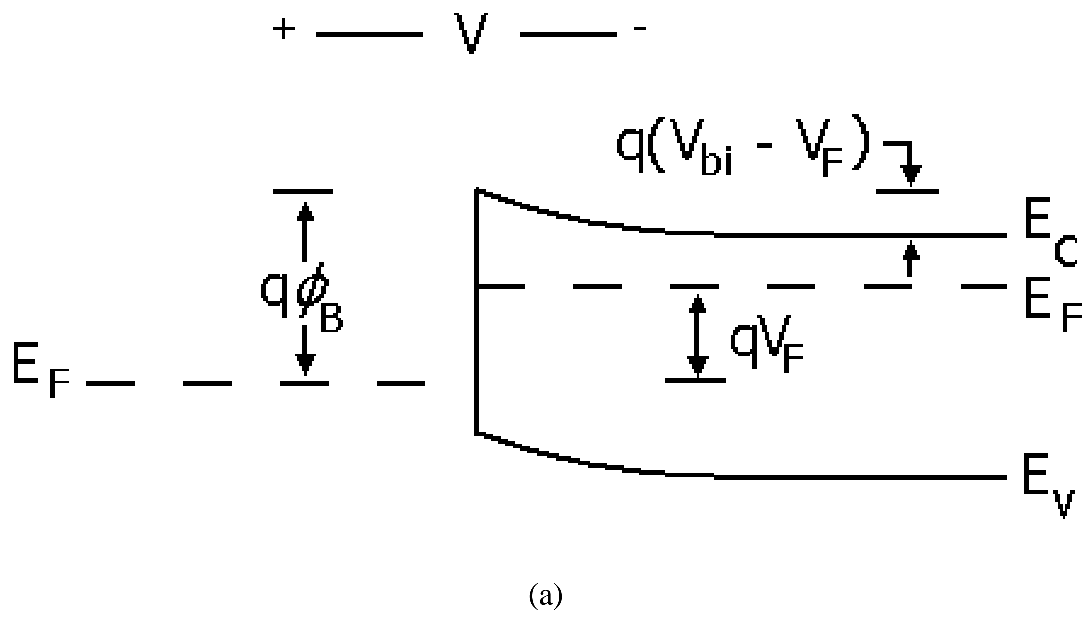

(a)

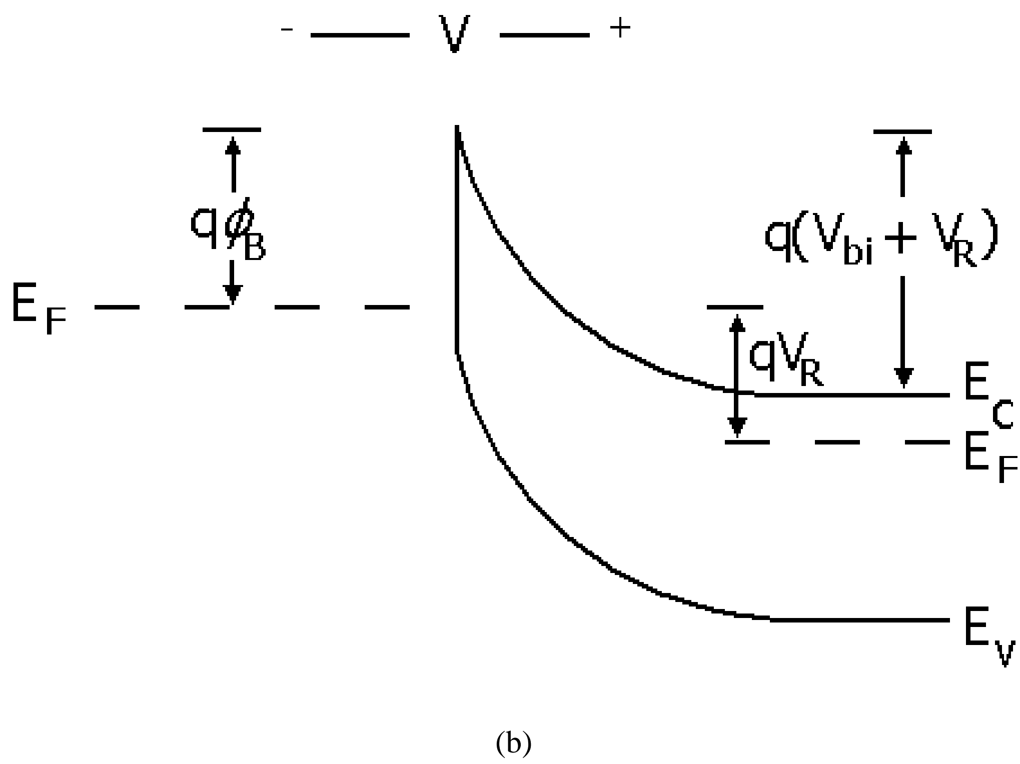

(b)

Fig. 6 Energy band diagram of a Schottky barrier illustrating the effects of applying (a) Forward bias (b) Reverse bias voltages [9].

2.3.2 Image force lowering

When a charge carrier (an electron) is brought close to the surface of a metal, it is attracted to the metal due to the induced electric field. This force is called image force and causes a lowering in the Schottky barrier, referred to as image force lowering. This is illustrated in Fig. 7. When the electron is brought close to the surface of the metal the electric field can be calculated as if there was a positive charge in the metal which is the same distance behind the metal-semiconductor interface as the electron is in front of the interface.

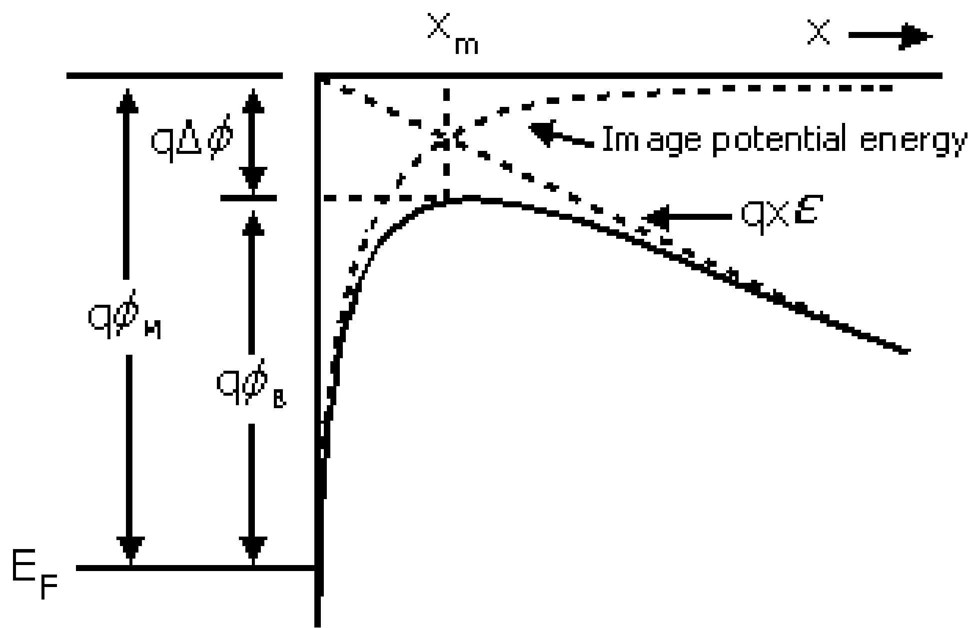

Fig. 7 Energy band diagram illustrating Schottky barrier lowering [9].

The force that the electron experiences as it approaches the metal can be written as

$$F = -\frac{q^2}{4\varepsilon_s\pi(2x)^2} = -\frac{q^2}{16\varepsilon_s\pi x^2} \tag{2.5}$$

where ε_s is the semiconductor permittivity which can be written as $\varepsilon_s = \kappa\varepsilon_o$. κ is the semiconductor dielectric constant while ε_o is the permittivity of the vacuum.

The potential energy of an electron brought from infinity to a distance x from the surface of the metal can be written as

$$U(x) = \int_{\infty}^{x} F \; dx = \frac{q^2}{16\varepsilon_s \pi x} \tag{2.6}$$

When an external electric field ξ is applied, the potential energy that the electron has can be written as

$$P(x) = \frac{q^2}{16\varepsilon_s \pi x} + q\xi x \tag{2.7}$$

To find the position where the electron will experiences the greatest potential energy, $P(x)$ is differentiated with respect to x and equated to zero such that the following equation represents that position:

$$x_m = \sqrt{\frac{q}{16\varepsilon_s \pi \xi}} \tag{2.8}$$

Substituting x_m into $P(x)$ gives the Schottky barrier lowering [9]:

$$\Delta\phi = \sqrt{\frac{q\xi}{4\varepsilon_s \pi}} = 2\xi x_m \tag{2.9}$$

Measurements of the barrier height which require the movement of electrons from the metal to the semiconductor and vice-versa depend on the image force lowering. Measurements like the capacitance measurements, which are dependent on the width of the space charge region, are not affected by the image-force lowering of the barrier height [15]. When a bias voltage is applied to a metal-semiconductor contact the Schottky barrier gets slightly affected. The barrier lowering can be quantified by $\Delta\phi_F$ and $\Delta\phi_R$ which represent the change in forward and reverse bias respectively as shown in Fig. 8.

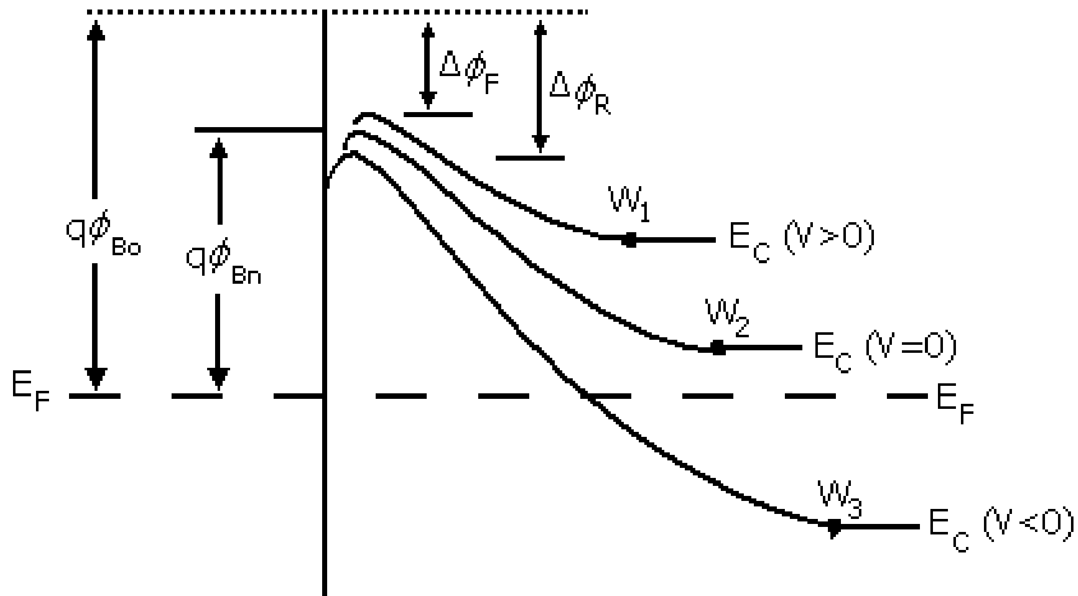

Fig. 8 Energy band diagram demonstrating Schottky lowering under different bias conditions [9].

2.3.3 Current transport mechanisms

The current associated with a metal-semiconductor contact is transported by majority carriers. There are a number of mechanisms which control the movement of electrons across a metal-semiconductor contact. These include: (1) the movement of electrons from the semiconductor over the Schottky barrier contact into the metal, (2) the quantum mechanical tunnelling of electrons through the barrier into the metal, (3) recombination of electrons and holes in the space-charge region, and (4) the recombination of electrons and hole in the neutral region. The last mechanism is the so called 'hole injection'. These mechanisms have been demonstrated schematically under forward bias in Fig. 9. A description of each mechanism is now explained.

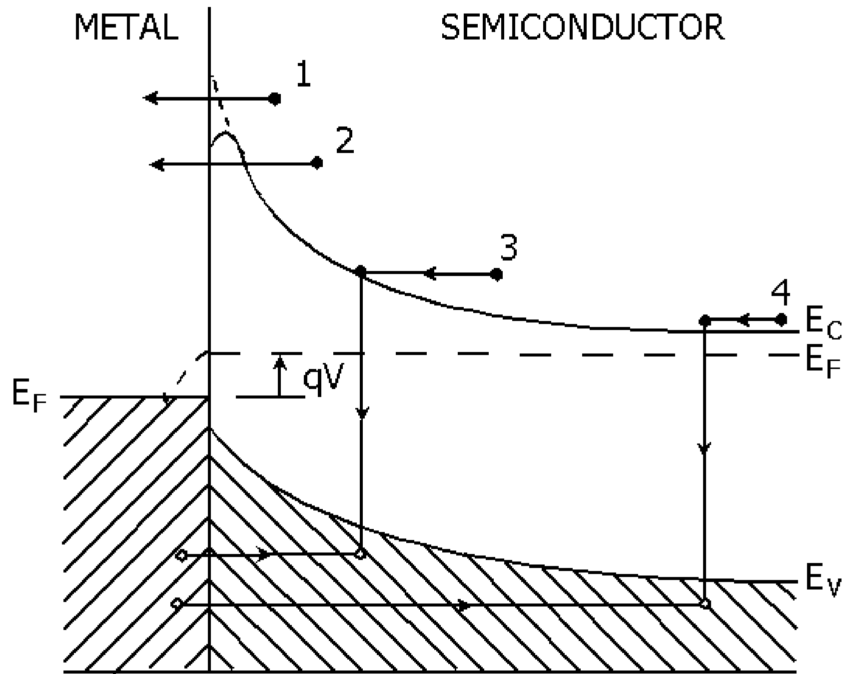

Fig. 9 Diagram showing different transport mechanisms that affect electron movement [15].

2.3.3.1 Thermionic emission

Current flow from the semiconductor into the metal in the thermionic emission model is solely dependent on the barrier height. Electrons from the semiconductor have to overcome the barrier height in order to flow into the metal. The current density of those electrons which are able to overcome the barrier height and flow into the metal is given by [9]:

$$J_{sm} = \int_{E_F + q\phi_B}^{\infty} q v_x \, dn \qquad (2.10)$$

where $E_F + q\phi_B$ is the minimum energy required for the electrons to overcome the barrier height and v_x is the carrier velocity in the direction of electron transport. The electron density in an incremental energy range is given by

$$dn = N(E)F(E)dE$$

$$= \frac{4\pi(2m^*)^{3/2}}{h^3}\sqrt{E - E_C}\exp\left[-\frac{E - E_C + qV_n}{kT}\right]dE \quad (2.11)$$

where $N(E)$ is the density of states, $F(E)$ the distribution function, m^* the effective mass of the semiconductor and qV_n is given by $E_C - E_F$. If we postulate that the energy of the electrons in the conduction band is kinetic energy, then

$$E - E_C = \frac{1}{2}m^*v^2$$

$$dE = m^*vdv$$

$$\sqrt{E - E_C} = v\sqrt{m^*/2} \quad (2.12)$$

After substituting equation (2.12) into (2.11), we get

$$dn = 2\left(\frac{m^*}{h}\right)^3 \exp\left(-\frac{qV_n}{kT}\right)\exp\left(-\frac{m^*v^2}{2kT}\right)(4\pi v^2 dv) \quad (2.13)$$

This equation gives the number of electrons per unit volume that have speeds between v and $v + dv$ distributed in different directions. If we were to resolve the speeds into different components whereby the electrons are transported parallel to the x axis, then

$$v^2 = v_x^2 + v_y^2 + v_z^2 \quad (2.14)$$

Utilising the transformation $4\pi v^2 dv = dv_x dv_y dv_z$ and substituting it into the above equations (2.10) and (2.13) we get

$$J_{sm} = \left(\frac{4\pi q m^* k^2}{h^3}\right)T^2 \exp\left(-\frac{qV_n}{kT}\right)\exp\left(-\frac{m^*v_{ox}^2}{2kT}\right) \quad (2.15)$$

where v_{ox} is the minimum velocity required to overcome the Schottky barrier in the x direction.

This velocity is given by

$$\frac{1}{2}m^{*}v_{ox}^{2} = q(V_{bi} - V) \quad (2.16)$$

Substituting equation v_{ox}^{2} into J gives

$$J_{sm} = \left(\frac{4\pi q m^{*} k^{2}}{h^{3}}\right) T^{2} \exp\left[-\frac{q(V_{n} + V_{bi})}{kT}\right] \exp\left(\frac{qV}{kT}\right)$$

$$= A^{*}T^{2} \exp\left(-\frac{q\phi_{B}}{kT}\right) \exp\left(\frac{qV}{kT}\right) \quad (2.17)$$

where ϕ_B is the barrier height and A^{*} is the effective Richardson constant for thermionic emission. This effective Richardson constant does not take into account the effects of optical phonon scattering and quantum mechanical reflection.

Electrons surmounting the barrier height from the metal to the semiconductor do not see a varying barrier and this implies that the current flowing into the semiconductor is not affected by an applied voltage. At thermal equilibrium, the current flowing from the metal to the semiconductor should be the same as that flowing from the semiconductor to the metal, that is, when V = 0. Therefore setting V = 0 in the above equation

$$J_{ms} = -A^{*}T^{2} exp\left(-\frac{q\phi_{B}}{kT}\right) \quad (2.18)$$

with the negative sign implying that the current is flowing from the metal to the semiconductor. The total current density flowing over the barrier is given by the sum of the current flow from the semiconductor into the metal and vice versa:

$$J_{tot} = \left[A^{*}T^{2} \exp\left(-\frac{q\phi_{B}}{kT}\right)\right]\left[\exp\left(\frac{qV}{kT}\right) - 1\right]$$

$$= J_{s}\left[\exp\left(\frac{qV}{kT}\right) - 1\right] \quad (2.19)$$

where

$$J_s = \left[A^* T^2 \exp\left(-\frac{q\phi_B}{kT}\right)\right] \tag{2.20}$$

is the saturation current density [9].

2.3.3.2 Quantum mechanical tunnelling

For a semiconductor that has high doping levels, the dominant current mechanism that can be observed at low temperatures is quantum mechanical tunnelling. The energy of some of the electrons that tunnel through the metal-semiconductor junction are close to the Fermi level of the semiconductor. Tunnelling at this level is referred to as field emission. When electrons have a higher energy level than the Fermi level, the barrier that they 'see' is much thinner. The tunnelling probability at this level becomes much greater than that of the field emission. This however means that fewer electrons will be able to reach this higher energy level where they can tunnel through the metal–semiconductor junction. Tunnelling at this level is referred to as thermionic-field emission. For the case where tunnelling is the dominant mechanism for current flow, the transmission coefficient is given by [16]:

$$T(\eta) \sim \exp\left(-\frac{q\phi_{Bn}}{E_{00}}\right) \tag{2.21}$$

where

$$E_{00} = \frac{q\hbar}{2}\sqrt{\frac{N_D}{\epsilon_s m^*}} \tag{2.22}$$

Comparing the energy E_{00} to the thermal energy kT, for $E_{00} \ll kT$ thermionic emission dominates, for $E_{00} \approx kT$ thermionic-field emission, and for field emission $E_{00} \gg kT$ [17]. The tunnelling current density can be expressed as [9]:

$$J_t \sim \exp\left(-\frac{q\phi_{Bn}}{E_{00}}\right) \tag{2.23}$$

For low doping levels tunnelling becomes more significant under reverse bias than forward bias because the bias voltages under reverse bias conditions are much greater. Under large

reverse bias voltages, the electrons in the semiconductor tunnel through the thin potential barrier into the metal [15].

2.3.3.3 Generation-recombination

Generation-recombination can be described as a condition through which electron hole pairs are created or destroyed. This can be described in two ways. The first is the band to band transition where an electron from the conduction band recombines with a hole in the valence band. The second can be described by localised states, which exist in the forbidden region within the space-charge region, that can either capture or emit electron and/or holes. Under reverse bias conditions, the dominant generation recombination process is the formation of an electron hole pair. A valence band electron is excited into an empty recombination centre. This electron is then excited into the conduction band. Fig. 10 depicts the recombination centres that can form in a semiconductor.

Under forward bias characteristics the dominant process is the destruction of an electron hole pair. This occurs when a conduction band electron loses energy and falls into an empty recombination centre and then into the valence band [10]. The most effective localised states are those that have energies which lie towards the centre of the forbidden gap of the semiconductor. This is because the recombination rate approaches a maximum at the centre of the forbidden gap. Current formed by recombination centres are the cause of the deviation of Schottky diodes from an ideal characteristic. This current is usually evident in materials with a high Schottky barrier and at low forward-bias voltage [9,15].

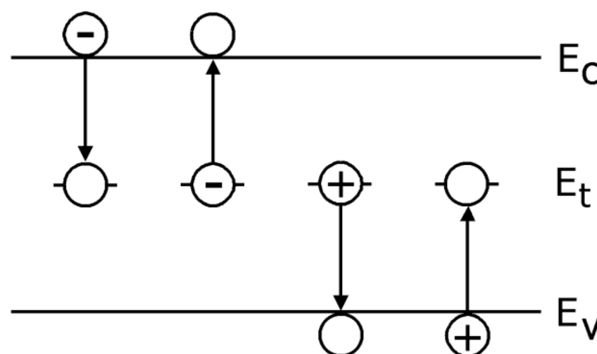

Fig. 10 Figure showing recombination centres in a semiconductor [9,10].

2.3.4 Electrical characterisation of Schottky barrier diodes

2.3.4.1 Introduction

A Schottky barrier is a barrier formed at a metal-semiconductor contact and is dependent on the metal work function, semiconductor electron affinity, and surface states. The expression of the Schottky barrier height is not as simplistic as the one given in equation (2.4). This expression assumes that the image force lowering effect and the surface state density are negligible. There are, however, cases in which the surface states play a role in the metal-semiconductor interface [18]. These may be represented by an energy level $q\phi_0$ which is coincident to the Fermi level before contact [19]. It shows the level at which the surface states must be filled in order for charge neutrality to be maintained at the surface. In the case where there are a large number of surface states, the Fermi level can be pinned at $q\phi_0$. This Fermi level pinning is a factor that causes the barrier height to be constant when various metals are deposited on a semiconductor. Fig. 11 is an energy diagram of the influences of different surface states on a Schottky barrier. If we take into account the effects of image force lowering and surface state density, the barrier height can be written as [18]

$$\phi_B = c_2(\phi_m - \chi) + (1 - c_2)\left(\frac{E_g}{q} - \phi_0\right) - \Delta\phi = c_2\phi_m + c_3 \tag{2.24}$$

where

$$c_2 = \frac{\epsilon_i}{\epsilon_i + q^2\delta D_s} \tag{2.25}$$

and δ the interfacial layer thickness, ϵ_i its permittivity and D_s the acceptor interfacial surface state density. The values of c_2 and c_3 can be determined experimentally which leads to

$$q\phi_0 = E_g - q\left(\frac{c_2\chi + c_3 + \Delta\phi}{1 - c_2}\right) \tag{2.26}$$

From the equation above (2.25)

$$D_s = \frac{(1 - c_2)\epsilon_i}{c_2\delta q^2} \tag{2.27}$$

Fig. 11 Schottky Barrier Height diagram with surface states [9].

If we use the assumption that the interfacial layer is thin, that is for a well-cleaned semiconductor substrate and that the permittivity of this layer can be approximated by the free space value, that is $\epsilon_i = \epsilon_0$, then

$$D_s \simeq 1.1 \times \frac{10^{13}(1-c_2)}{c_2} \quad \frac{\text{states}}{\text{cm}^2 \cdot \text{eV}} \tag{2.28}$$

For $D_s \rightarrow \infty$ and $c_2 \rightarrow 0$

$$q\phi_B = \left(E_g - q\phi_0\right) - q\Delta\phi \sim \frac{2}{3}E_g \tag{2.29}$$

This equation implies that in this case the barrier height is independent of the metal work function and dependent on the doping and surface properties of the semiconductor.

Where the semiconductor is independent of the metal work function, the barrier height is equal to about two thirds of the bandgap energy. This is due to the fact that looking at a number of metals deposited on semiconductor substrates (including group III nitrides) [18], the value of $q\phi_0$ was close to a third of the bandgap [9]. For a case where D_s is negligible, c_2 approaches 1, and the barrier height is given by

$$q\phi_B = q(\phi_m - \chi) - q\Delta\phi \tag{2.30}$$

There are two methods for the measurement of the barrier height of a metal-semiconductor diode that will be discussed. These are the current-voltage and capacitance-voltage methods [20].

2.3.4.2 Current-voltage

The ideal *I-V* characteristics are based on a number of assumptions namely that the boundaries of the depletion region are abrupt and the semiconductor is neutral outside of these boundaries, the Boltzmann approximation is valid, the majority carriers are much greater than the minority carriers, and no generation current exists in the depletion region [9]. Frequently, for slight deviations from ideality, the current voltage relationship of a Schottky diode for thermionic emission is given by [15]:

$$J = J_s \{\exp(qV/nkT) - 1\} \tag{2.31}$$

where J_s is the saturation current

$$J_s = A^* T^2 \exp\left(-\frac{q\phi_B}{kT}\right) \tag{2.32}$$

and n is the ideality factor given by

$$\frac{1}{n} = \frac{kT}{q}\frac{d(\ln J)}{dV} \tag{2.33}$$

A^* in the above equation is the Richardson constant

$$A^* = \frac{4\pi m^* q k^2}{h^3} = 120\frac{m^*}{m}\left(\frac{AK^2}{cm^2}\right) \tag{2.34}$$

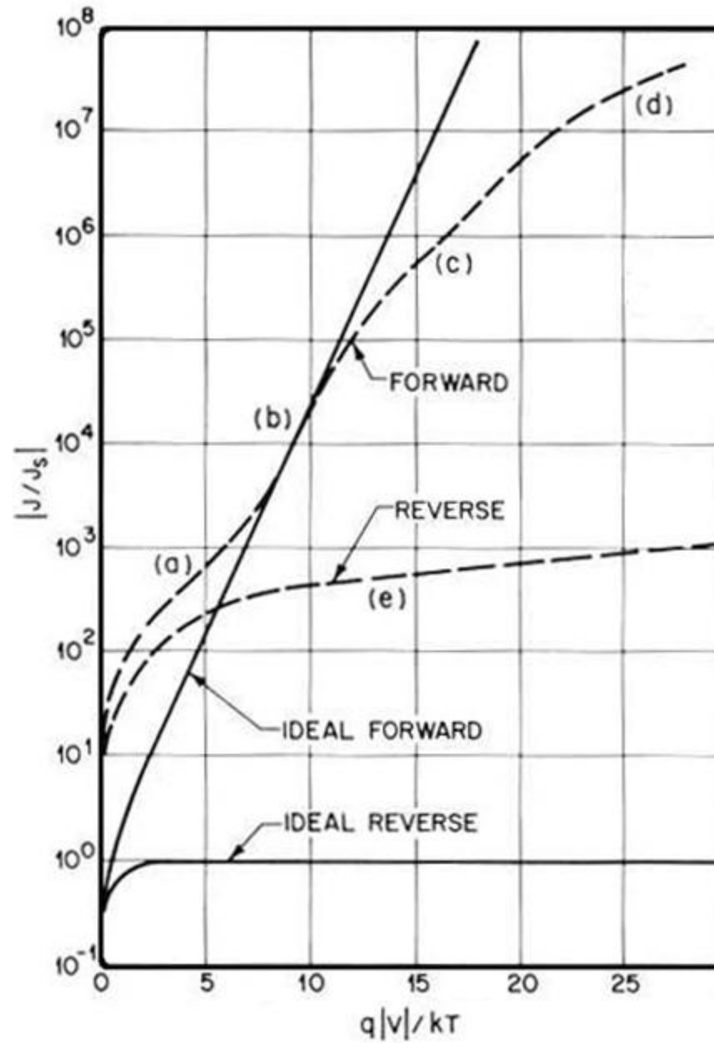

Fig. 12 *I*-*V* characteristics of a Schottky diode (a) generation recombination (b) thermionic emission (c) hole injection (d) series resistance (e) reverse current leakage [9].

The ideality factor is a measure how much the forward characteristics of a Schottky diode deviates from the ideal case, for which the ideality factor is equal to unity. A non ideal diode is one whose ideality is much greater than unity. The factors that can cause a diode to depart from ideality include surface effects which are due to ionic charges on the semiconductor surface that induce image charges in the semiconductor, series resistance, and the transport mechanisms described above, namely generation-recombination, tunnelling and high injection [9]. Fig. 12 is a diagram of the *I*-*V* characteristics that are evident for an ideal and a non-ideal Schottky diode. The Schottky barrier height can thus be determined by the equation

$$\phi_B = \frac{kT}{q} ln\left(\frac{A^{**}T^2}{J_s}\right) \tag{2.35}$$

2.3.4.3 Capacitance-voltage

The capacitance in a Schottky diode is mainly due to the change in the charge in the depletion region. These charges come from three sources. The positive charges can be attributed to uncompensated donors in the depletion region and holes in the valence band. The negative charges are due to electrons on the surface of the metal. If a reverse bias voltage is applied, the width of the depletion region increases and the current in the region changes. The contributing factors to this total current include the displacement current and the conduction current. The displacement current is caused by the change in the electric field in the depletion region. The conduction current is due to two factors namely electrons being emitted over the metal-semiconductor barrier and electrons and holes flowing out of the depletion region. The former occurs at constant bias voltage (time independent) and constitutes the reverse current but the latter arises as the negative bias voltage is increased (time dependent) [15].

When measuring the capacitance, a constant direct current (DC) bias voltage is applied to the diode. A small alternating current (AC) voltage is then superimposed on the DC voltage and the AC measured. The depletion region of a Schottky barrier can be modelled in some respects to a parallel plate capacitor with the depletion region acting like an insulator. The capacitance of a parallel plate capacitor is given by the following equation [21]

$$C = \frac{\kappa \varepsilon_0 A}{W} \tag{2.36}$$

where κ is the dielectric constant of the semiconductor, ε_0 the permittivity constant, A the area of the diode and W the depletion width. The depletion width of a metal-semiconductor is given by [9]

$$W(V) = \sqrt{\frac{2\kappa\varepsilon_0}{qN_d}\left(V_{bi} - V - \frac{kT}{q}\right)} \tag{2.37}$$

where N_d is the donor impurity density (carrier density), V_{bi} the built-in voltage, V the bias voltage, and k the Boltzmann's constant.

If we substitute equation *W(V)* into *C* we get

$$C = \sqrt{\frac{q\kappa\varepsilon_0 A^2 N_d}{2\left(V_{bi} - V - \frac{kT}{q}\right)}} \tag{2.38}$$

This is usually written in the form

$$\frac{1}{C^2} = \frac{2\left(V_{bi} - V - \frac{kT}{q}\right)}{q\kappa\varepsilon_0 A^2 N_d} \tag{2.39}$$

The above equation can be modelled as that of a straight line. From it the slope that is obtained is given by $-2/q\kappa\varepsilon_0 A^2 N_d$. When plotting $1/C^2$ versus V, a straight line implies that the carrier density N_d is constant. The doping profile can be obtained by using the differential capacitance method when $N_{d.}$ is not a constant. This can be done by differentiating equation $1/C^2$ so that

$$-\frac{d(\frac{1}{C^2})}{dV} = \frac{2}{q\kappa\varepsilon_0 A^2 N_d} \tag{2.40}$$

or

$$N_d = \frac{2}{q\kappa\varepsilon_0 A^2}\left[-\frac{1}{d(\frac{1}{C^2})/dV}\right] \tag{2.41}$$

Once N_d has been obtained, then V_{bi} can be determined from the $1/C^2$ intercept. V_{bi} can also be determined from the V intercept V_i where $V_i = V_{bi} - kT/q$. The barrier height can be obtained from the following equation:

$$\phi_B = V_i + V_n + \frac{kT}{q} \tag{2.42}$$

where V_n is the energy difference between the Fermi level below the conduction band [9].

2.3.5 Ohmic contact

An ohmic contact is formed when a metal and a semiconductor are brought into contact with each other by which the work function of the (n-type) semiconductor is greater than that of the metal $\phi_s > \phi_m$. Electrons in the metal will flow into the semiconductor until thermal equilibrium is reached, when the Fermi levels align. The conduction and valence bands in the semiconductor will bend as shown in Fig. 13. This will create an 'accumulation region' which has quite a high concentration of electrons [15]. A good ohmic contact should be able to allow current to flow easily across the metal-semiconductor contact in either direction. This type of contact will have negligible contact resistance when compared to the bulk of the semiconductor [9,22]. An alternative method to form an ohmic contact is to highly dope the region under the contact so that tunnelling becomes the dominant current transport mechanism.

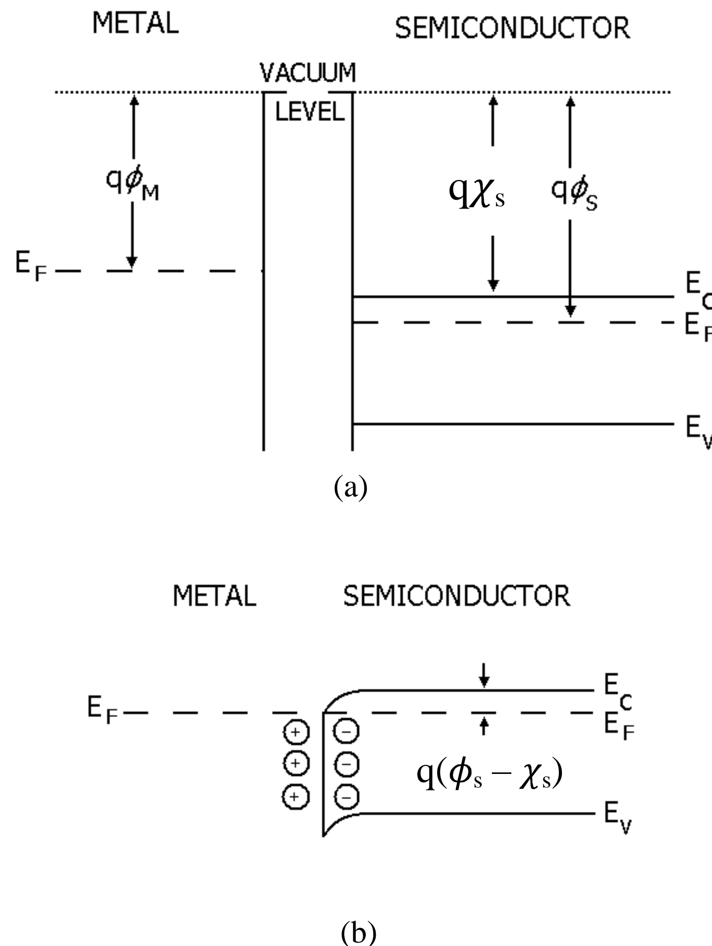

Fig. 13 The energy bands of a metal and semiconductor forming an ohmic contact: (a) before contact (b) after contact.

An ohmic contact is usually characterised in terms of the specific contact resistance R_c given by the following equation

$$R_c = \left(\frac{\partial J}{\partial V}\right)^{-1}_{V=0} \tag{2.43}$$

where the specific contact resistance is evaluated at zero bias. For lowly doped semiconductors, the dominant transport mechanism is thermionic emission whereas for highly doped semiconductors the dominant mechanism is tunnelling.

2.3.6 Photonic devices

2.3.6.1 Introduction

Photonics is a study of the photon and its applications. This can include generation, transmission or detection of photons. There are a number of devices which can be manufactured with regards to this and these include light emitting diodes (LEDs), photodetectors and solar cells. LEDs are devices that convert electrical signal into optical radiation. They are formed when electrons in the conduction band recombine radiatively with holes in the valence band. When the junction is forward biased, photons are emitted. This process is usually only efficient in direct bandgap semiconductors. The colour of the light will depend on the material that is used. Solar cells convert an optical signal into electrical energy. These solar cells can be used in solar batteries or solar panels. Photodetectors are devices that are used to detect optical radiation by electronic processes. In this study the UV range is studied. The sun is a huge source of UV radiation. UV radiation can be classified into three categories according to its effect on the biosphere. UV-A corresponds to the 400 – 320 nm wavelength range (3.1 to 3.87 eV) and causes premature aging. UV-B corresponds to 320 – 280 nm (3.87 to 4.43 eV) and causes skin cancer. UV-C, which is the most energetic and most dangerous, corresponds to 280 – 10 nm (4.43 to 124 eV). The latter is usually referred to as the solar blind region [23,24,25]. Another classification that has been widely used is: near UV (400 – 300 nm), middle-UV (300 – 200 nm), far-UV (200 – 100 nm) and extreme UV (100 – 10 nm) [23]. We now discuss photodetectors.

2.3.6.2 Photodetectors

Photodetectors as described above are electronic devices that respond to an optical signal (light) by means of electronic processes. The processes that are relevant to the operation of such a device include the generation of carriers by incident light, the transportation of the carriers and the generation of an output signal. These photodetectors need to have low noise, be sensitive to radiation at desirable wavelengths, have low dark currents when reverse bias voltages are applied, and must have high response speeds. There are a number of photodetectors that can be investigated which include: photoconductors, metal-semiconductor-metal, phototransistor and the photodiode. Fig. 14 shows the metal layers of these devices. In this study we will investigate the photodiode.

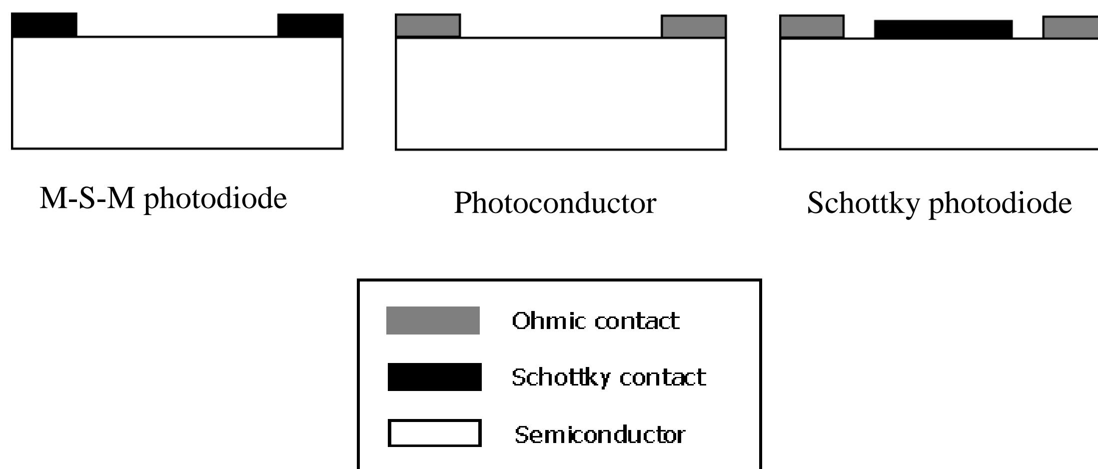

Fig. 14 A diagram showing different photodetectors [26].

2.3.6.3 Photodiodes

There are different types of photodiodes that can be considered which include p-n junction diode, p-i-n diode, Schottky diode and heterojunction diode. The three main parameters of a photodiode are quantum efficiency, response speed and device noise (there's a trade-off between response speed and the quantum efficiency). For the purpose of this research, the quantum efficiency will be investigated. The quantum efficiency (also called the quantum

yield) is a measure of the efficiency of incident electromagnetic radiation to produce a reaction from the receptive device by creating electron-hole pairs. The equation is given by:

$$\eta = \frac{\frac{I_p}{q}}{\frac{P_{opt}}{h\nu}} \tag{2.44}$$

where I_p is the photocurrent generated by the absorption of an incident light with optical power P_{opt} that has photon energy hv. For an ideal photodiode, $\eta = 1$. The absorption coefficient plays a key role in determining the quantum efficiency. The responsivity is given as the ratio of the photocurrent to the optical power:

$$R = \frac{I_p}{P_{opt}} = \frac{\eta q}{h\nu} = \frac{\eta\lambda\,(\mu\text{m})}{1.24} \qquad \frac{\text{A}}{\text{W}} \tag{2.45}$$

2.3.6.4 Schottky photodiode

The metal on a Schottky photodiode has to be so thin that incident light can be transmitted through it to the metal-semiconductor junction. An antireflection coating is at times deposited to avoid reflection losses. There are a number of modes that the Schottky photodiode can be operated. These are in essence dependent on the energy of the photons and the biasing conditions. The three modes are now explained. The energy band diagrams of these are shown in Fig. 15.

a. $E_g > hv > q\phi_B$ and $V < V_B$, where V_B is the avalanche breakdown voltage. In this case the electrons in the metal are exited in such a way that they are able to overcome the barrier height and flow into the semiconductor [27].

b. $hv > E_g$ and $V < V_B$. The current is produced from electron-hole pairs in the semiconductor created by light shone onto the Schottky contact that is greater than the bandgap

c. $hv > E_g$ and $V \approx V_B$. This situation is usually considered for avalanche photodiodes. These kinds of diodes are operated at high reverse bias voltage where there is high internal current gain [9].

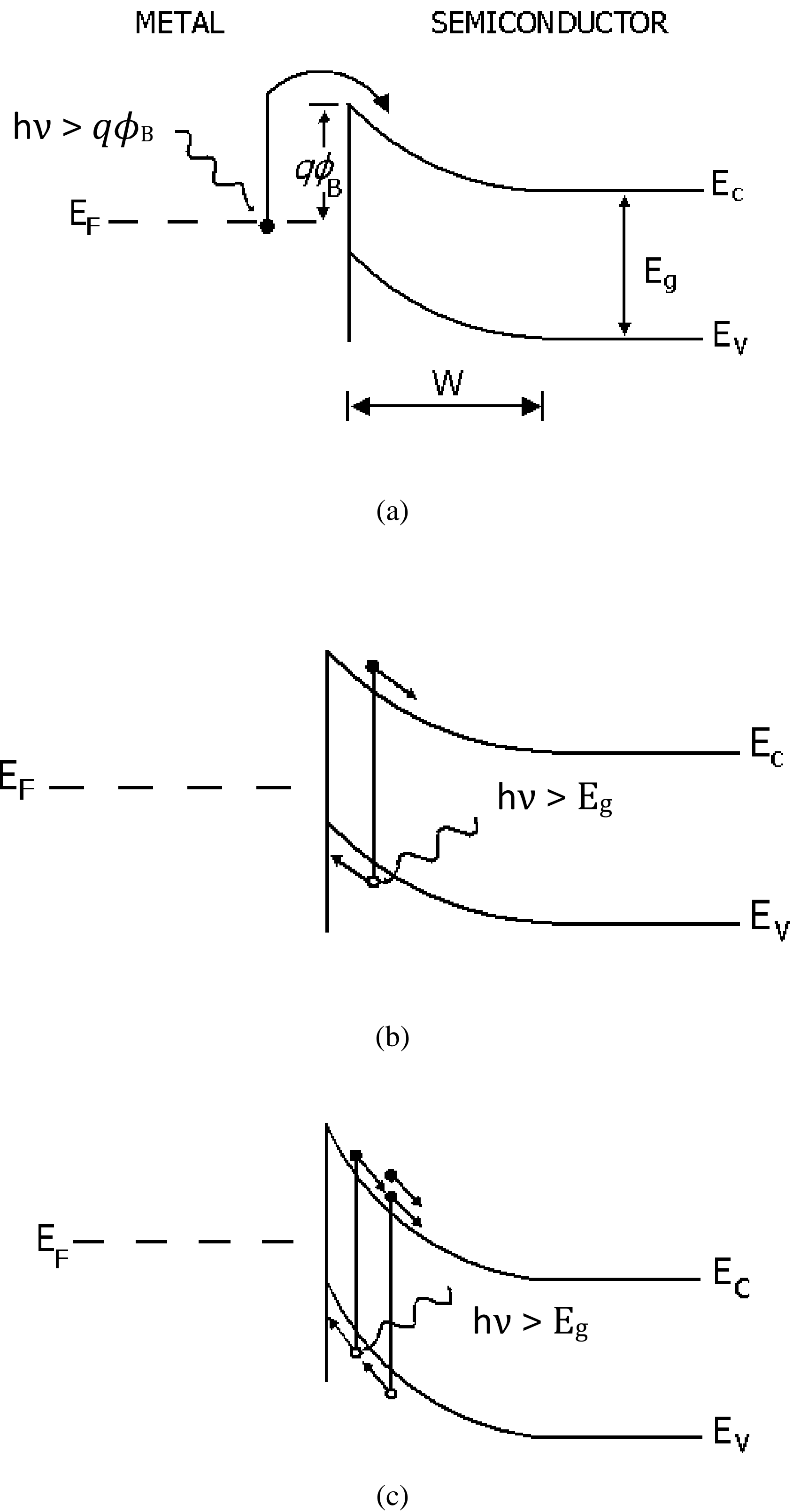

Fig. 15 Energy band diagrams showing different modes under which a Schottky photodiode operates [9].

The Schottky photodiode operates within a certain wavelength range depending on the semiconductor that is being used. There exists a wavelength above which the photodiode is not responsive. This wavelength is called the cut-off wavelength and defined by:

$$\lambda_c = \frac{hc}{E_g} = \frac{1.24}{E_g\ (eV)}\ (\mu\text{m}) \tag{2.46}$$

where h is Planck's constant and c is the speed of light.

REFERENCES

[1] S.N. Mohammad and H. Morkoç, Prog. Quant. Electr. **20** (5/6), (1996) 361.

[2] M. Palczewska and M. Kamińska, "Magnetic resonance studies of defects in GaN and related compounds", in O Manasreh (ed.), *III-Nitride semiconductors: electrical, structural and defects properties*, Elsevier Science B.V., Amsterdam, 2000.

[3] K. E. Miyano, J.C. Wojcik, L.H. Robins, C.E. Bouldin, and D.E. Wickden, Phys. Rev. B **45**, (1992) 83.

[4] M. Schmidt, "Space charge spectroscopy applied to defect studies in ion-implanted zinc oxide thin films" PhD Thesis, University of Leipzig, 2012.

[5] F. Yun, M.A. Reshchikov, L. He, T. King, H. Morkoç, S.W. Novak, and L. Wei, J. Appl. Phys. **92** (8), (2002) 4837.

[6] L. Van Schalkwyk, "Development of an opto-electrical system for the characterisation of UV photodiodes", BSc Hons (Physics) Project (unpublished), University of Pretoria, 2009.

[7] S.J. Pearton, F. Ren, A.P. Zhang, and K.P. Lee, Mater. Sci. and Eng. **R30**, (2000) 55.

[8] B.G. Streetman and S. Banerjee, Solid State Electronic Devices, Prentice Hall, New Jersey, 2000.

[9] S.M. Sze, Physics of Semiconductor Devices, John Wiley and Sons, New York, 1981.

[10] K.A. Jones, Introduction to Optical Electronics, John Wiley and Sons, New York, 1987.

[11] T.F. Kuech and M.A. Tischler, "Epitaxial Growth", in K.A. Jackson and W. Schröter (eds.), *Handbook of Semiconductor Technology vol. 1-2*, John Wiley and Sons, New Yok, 2000.

[12] M.S. Tyagi, Introduction to Semiconductor Materials and Devices, John Wiley and Sons, New York, 1991, pp 134-136, 141-142, 283-284, 579, 592-594.

[13] S. Denbaars, Proc. of IEEE **11**, (1997) 1740.

[14] Dictionary of physics, Longman Group, London, 2000.

[15] E.H. Rhoderick and R.H. Williams, Metal-Semiconductor Contacts, 2nd ed., Clarendon Press, Oxford, 1988.

[16] F.A. Padovani and R. Stratton, Solid State Electron. **9**, (1969) 695.

[17] D. K. Schroder, Semiconductor Material and Device Characterization, John Wiley and Sons, New York, 1998.

[18] S.S. Li, “Semiconductor Physical Electronics” (2nd ed,), Springer, New York, 2006.

[19] J. Bardeen, Phys. Rev. **71**, (1947) 717.

[20] C.A. Mead, Solid State Electron. **9**, (1966) 1023.

[21] D. Halliday, R. Resnick, and J. Walker, Fundamentals of Physics, John Wiley and Sons, New York, 2001.

[22] A.G. Milnes and D.L. Feucht, Heterojunctions and metal-semiconductor junctions, Academic Press, New York, 1973.

[23] E. Monroy, Semicond. Sci. Technol. **18**, (2003) R33.

[24] E. Muñoz, E. Monroy, J.L. Pau, F. Calle, E. Calleja, F. Omnès, and P. Gibart, Phys. Stat. Sol. (a) **180** (2000) 29.

[25] F. Omnès, E. Monroy, E. Muñoz, and J.L. Reverchon, Proc. of SPIE **6473**, (2007) 64730E-1.

[26] E. Monroy, F. Calle, J.L. Pau, E. Muñoz, F. Omnès, B. Beaumont, and P. Gibart, J. Cryst. Growth **230**, (2001) 537.

[27] C.R. Crowell, W.G. Spitzer, L.E. Howarth, and E.E. Labate, Phys. Rev. **127** (6), (1962) 2006.

CHAPTER 3

EXPERIMENTAL TECHNIQUES

3.1 INTRODUCTION

In this chapter the experimental techniques used in this work are explained. Firstly the sample preparation is described. In section 3.3 the metal deposition techniques are explained. These include the electron beam and the resistive evaporation systems. The former was used to deposit both ohmic and Schottky contacts while the latter was used only for fabricating Schottky contacts. After the deposition the contacts were thermally annealed. The annealing techniques as well as the apparatus are described in section 3.4. Finally, the electrical and optical characterisation of the samples concludes the chapter. The electrical characterisation includes performing *I-V* and *C-V* measurements from which parameters such as the Schottky barrier height and ideality factor were determined. The optical measurements of the Schottky photodiodes and the metal layers include photocurrent and transmission measurements respectively. The photocurrent measurements include irradiating the metal-semiconductor interface with light and measuring the induced photocurrent. In the transmission section the transmittance of light through the Schottky contact metal multilayer as deposited on a quartz substrate is presented.

3.2 SAMPLE PREPARATION

In order to produce a low reverse current and high barrier height, the surface of the wafer on which the device is produced has to be free from contaminants. A chemical and mechanical treatment of the wafers plays a critical role in achieving this cleanliness. There are two types of cleaning that can be described namely liquid and dry cleaning. Dry cleaning refers to the mechanical cleaning of a sample. The samples used in this experiment were cleaned using the liquid cleaning method. The first step in the cleaning process was degreasing, thus organic chemicals were used as solvents for the removal of any organic residues. This is necessary

because organic residues on the wafer surface could react and diffuse into the semiconductor material under heat treatment to form defects leading to traps or generation-recombination centres in the forbidden region [1]. The AlGaN wafers were firstly boiled in trichloroethylene and then rinsed in isopropanol. Each of the dips lasted 3 minutes. Once this had been done the second phase of cleaning, namely etching, was performed. HCl based solutions are known to be successful in removing surface oxides [2]. The wafers were submerged into boiling aqua regia for 10 minutes and an HCl:H_2O (1:1) solution for 1 minute. The cleaning of GaN based materials with Cl containing chemicals, in particular HCl, has been known to produce a substrate onto which adhesion of metals is enhanced [3]. In between all the chemical cleaning steps deionised water was used to rinse off the chemicals and organic residue and this was done in an ultrasonic bath. Once all the cleaning steps had been completed, the wafers were blow dried by nitrogen in order to remove any remaining liquid.

3.3 DEPOSITION

There are various ways to achieve metal-semiconductor contacts which include electroplating, sputtering, alloying and evaporation. The metal depositions in this study were accomplished using two systems namely the electron beam and the resistive evaporator systems. The electron beam system was used to carry out the deposition of the ohmic contacts. The ohmic contact required 4 different metal layers namely Ti/Al/Ni/Au. This metal contact scheme is known to produce an ohmic contact of low contact resistance [4]. Luther *et al*. [5] have proposed that at higher temperatures the Al diffuses through the Ti to improve the ohmic contact. It has also been suggested that the formation of a TiN layer formed from the Ti and N causes a decrease in the contact resistance especially after annealing. Furthermore, a thick enough Al layer prevents the outdiffusion of Ga to the Au layer. The Ni/Au layer is deposited in order to prevent the oxidation of the Al which can increase resistivity [6].

The thicknesses of the metals forming the ohmic contact were as follows: Ti (150 Å)/ Al (2200 Å)/ Ni (400 Å)/ Au (500 Å). The thicknesses of the Schottky contacts deposited on the samples were either 70 Å or 100 Å. The metal schemes for the Schottky contacts deposited on the samples were Ni (50 Å)/ Au (50 Å), Ni (20 Å) / Au (50 Å), and Ni (20 Å)/ Ir (30 Å)/ Au (50 Å). This was because the samples were being prepared to form Schottky photodiodes

which needed a thin metal layer so that radiated light would be able to reach the metal-semiconductor contact where the light would be absorbed by the semiconductor to produce a photocurrent. The holes on the Schottky mask had a 0.6 mm diameter. A schematic of the way in which the Ohmic and Schottky contacts were deposited can be seen in Fig.1.

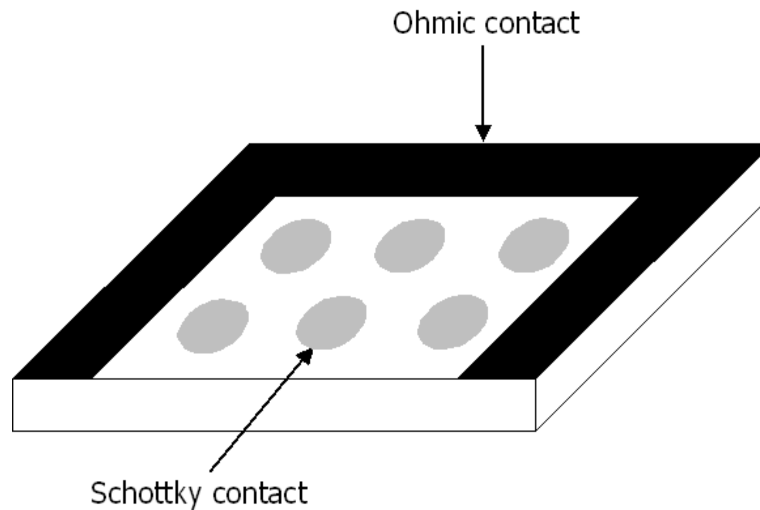

Fig. 1 Schottky photodiode composed of different metal contacts on an AlGaN substrate.

3.3.1 Electron beam system

All the ohmic contacts were deposited consecutively in the electron beam system shown in Fig. 2. This system has the capacity to deposit all four metals of the ohmic contact without having to break vacuum. The electron beam system can be used to melt metals that have a high melting point due to its ability to reach high power. This system was also used to deposit the Schottky contact requiring a three metal layer scheme namely the Ni/Ir/Au metal layer. The air in the chamber was first pumped out to pressures of around 2.5×10^{-2} mbar with a rotary pump. At this pressure the turbo molecular pump was switched on. The metals in the electron beam system were deposited at pressures of about 1.3×10^{-4} mbar. The deposition rates for depositing the metals were between 0.2 and 0.5 Å/s.

3.3.2 Resistive evaporator system

A rotary pump was firstly used to pump out the air in the bell jar of the resistive evaporator system until the pressure was about 2×10^{-4} mbar. At this pressure the turbo pump was

switched on and it pumped out the air until the pressure was about 4×10^{-5} mbar. This was an appropriate pressure to start the deposition. The appropriate metal was melted in a crucible and then evaporated onto the semiconductor which had been mounted onto the Schottky mask. The thicknesses of the evaporated metals were monitored by an Inficon XTC monitor. The deposition rate for the evaporation of Ni and Au was between 0.2 and 0.5 Å/s. A picture of the resistive evaporator system that was used is shown in Fig. 3.

Fig. 2 A picture of the electron beam system.

Fig. 3 A picture of the resistive evaporation system.

3.4 ANNEALING

A Lindberg annealing furnace as depicted in Fig. 4 was used for all the required annealing. It had the ability to reach temperatures of up to 1200 ^{o}C. Refractory bricks were lined up on the inside of the furnace in order to minimise heat from being dissipated out of the furnace. The samples were placed in a quartz tube and annealed under a flowing Argon atmosphere as it is an inert gas. The flow rate of the argon gas was 2 litres per minute. The ohmic contacts were not annealed prior to the deposition of the Schottky contacts. The Schottky contacts were annealed at 200, 300, 400, and 500 ^{o}C. The time taken at each annealing temperature was 5 minutes. After each annealing step the photodiodes were electrically and optically characterised.

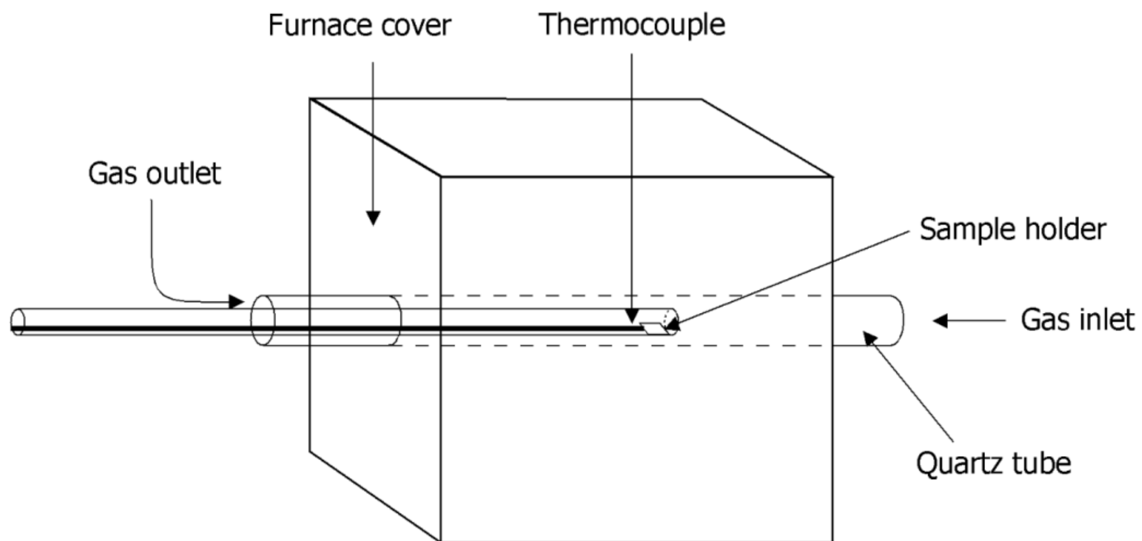

Fig. 4 Schematic diagram of a Lindberg furnace.

3.5 MEASUREMENT TECHNIQUES

3.5.1 Electrical characterisation

The electrical properties of the devices were investigated by current-voltage (*I*-*V*) and capacitance-voltage (*C*-*V*) measurements conducted in a dark metal enclosure in order to

avoid any external influence by light or stray electric and magnetic fields. The *I-V* measurements were performed using an HP 4140B pA Meter/DC Voltage Source. These were done after each annealing step. The measurements included the forward and reverse currents and the parameters that were extracted from these measurements were the Schottky barrier height, ideality factor, and series resistance. The *C-V* measurements were performed using an HP 4192 A LF Impedance Analyser. The Schottky barrier height was determined from these *C-V* measurements. All the electrical characterisations of the Schottky photodiodes were performed using a LabView™ routine.

3.5.2 Optical characterisation

3.5.2.1 Photocurrent measurements

The setup used for the photocurrent measurements was the same as the one used for *I-V* and *C-V* measurements. The difference between the two setups is that a monochromator and light source were added to the *I-V* and *C-V* station in order to illuminate the sample with monochromatic light allowing photocurrent measurements to be performed. The monochromator used for this experiment was a Digikrom DK 240 1/4 meter monochromator which was connected to a 30 W deuterium lamp. The monochromator was connected to an optical fibre which guided the light to the photodiode that was being characterised. Fig. 5 shows a diagram of this setup. The connection between the monochromator and the *I-V/ C-V* station in Fig. 5 depicts the optical cable while the rest are all electrical cables. Before any characterisation of the samples could be made, the irradiance of the monochromator had to be calibrated. This was done using a calibrated Si-based detector.

Fig. 6 shows a typical irradiance spectrum measured for the purpose of calibrating the monochromator. All the measurements were performed using a LabView™ routine. The two important parameters that were extracted from the photocurrent measurements were the quantum efficiency and the responsivity.

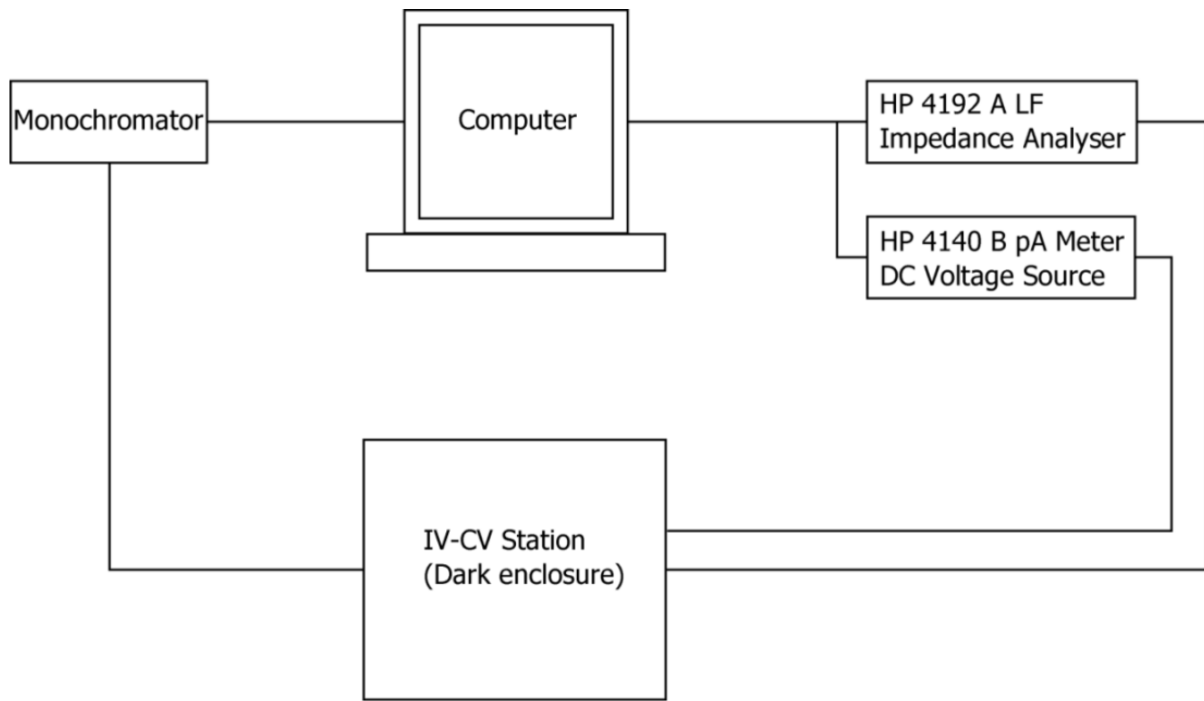

Fig. 5 Schematic diagram of the *I-V* and *C-V* station setup with the monochromator.

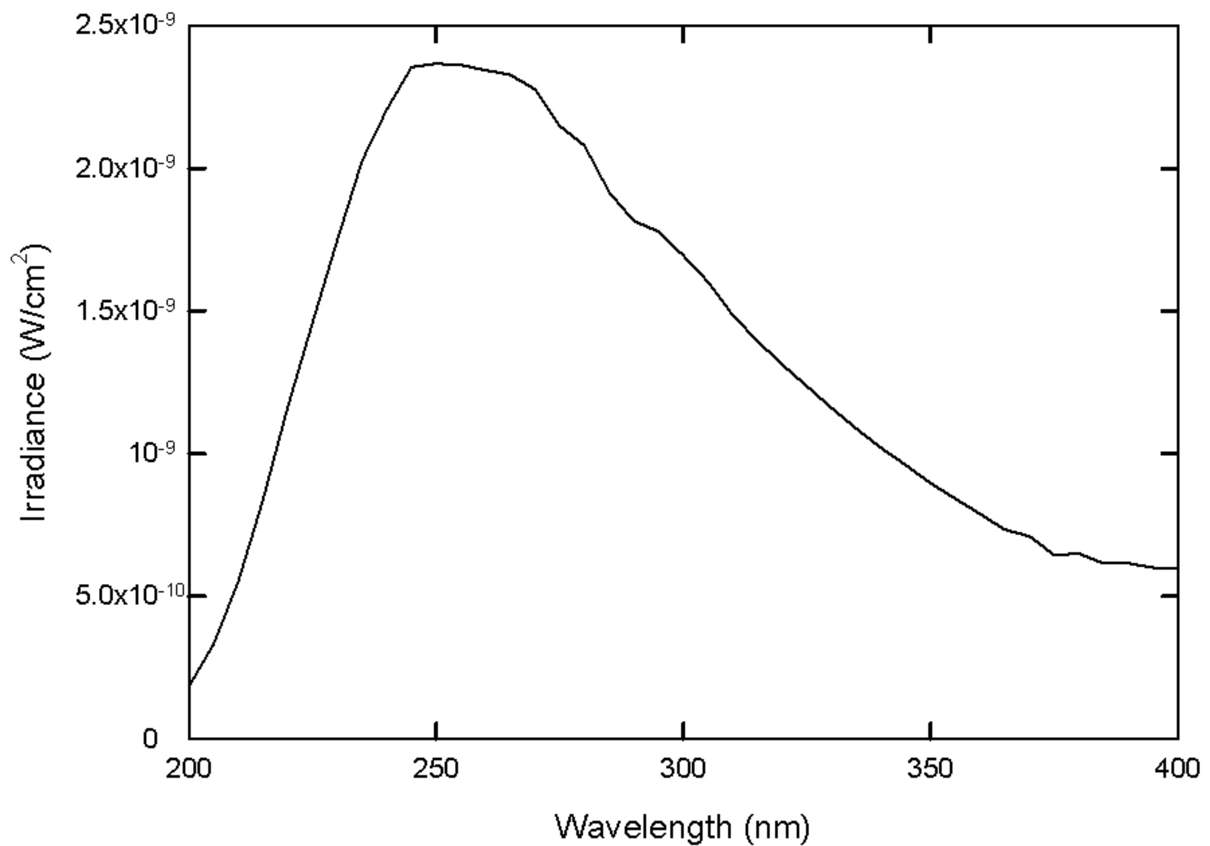

Fig. 6 The calibrated irradiance spectrum of the Digikrom monochromator

3.5.2.2 Transmission measurements

The transmittance measurements required that the same metal schemes used for the Schottky photodiodes be deposited onto a 6 × 6 mm quartz substrate. The substrates had to be degreased by firstly dipping them into trichloroethylene and methanol, and then rinsing them in de-ionised water. Lastly they were blown dry by N_2. The layer thicknesses of the metals used for transmission measurements corresponded to the thicknesses used for the Schottky contacts. Ni (50 Å)/ Au (50 Å) and Ni (20 Å)/ Au (50 Å) metals were deposited using the resistive evaporation system whilst the Ni (20 Å)/ Ir (30 Å)/ Au (50 Å) metals were deposited utilising the electron beam system. The transmission measurements were done using a Perkin Elmer Lambda 25 UV/VIS Spectrometer. During the measuring process the transmittance had to be normalised with respect to the quartz substrate. The samples were annealed under the same conditions as the Schottky photodiodes, that is, in an Ar ambient, and at temperatures 200, 300, 400, and 500 ^{o}C.

REFERENCES

[1] W. Kern, *Handbook of semiconductor wafer cleaning technology – science, technology and applications*, (Noyes publications, Westwood), 1993.

[2] L.L. Smith, S.W. King, R.J. Nemanich, and R.F. Davis, J. Electron. Mater. **25**, (1996) 805.

[3] M. Diale, F.D. Auret, N.G. van der Berg, R.Q. Odendaal, and W.D. Roos, Appl. Surf. Sci. **246**, (2005) 279.

[4] B. Boudart, S. Trassaert, X. Wallart, J.C. Pesant, O. Yaradou, D. Theron, Y. Crosnier, H. Lahreche, and F. Omnes, J. Electron. Mater. **29** (5), (2000) 603.

[5] B.P. Luther, S.E. Mohney, T.N. Jackson, M. Asif Khan, Q. Chen, and J.W. Yang, Appl. Phys. Lett. **70** (1), (1997) 57.

[6] Z. Fan, S.N. Mohammad, W. Kim, O. Aktas, A.E. Botchkarev, and H. Morkoç Appl. Phys. Lett. **68** (12), (1996) 1672.

CHAPTER 4

RESULTS AND DISCUSSION 1

4.1 INTRODUCTION

This chapter discusses the optical and electrical characteristics of a Ni (50 Å)/ Au (50 Å) Schottky photodiode and the evolution of these characteristics with increasing annealing temperature. The electrical properties included *I*-*V* and *C*-*V* characteristics while the optical properties were the responsivity of the photodiode and transmittance of the metal layer.

4.2 EXPERIMENTAL

The cleaning procedures for GaN based materials have been established [1]. The wafers were cleaned by a two-step process which included degreasing and etching. Degreasing was done by dipping the sample into two separate organic solutions isochronously for 3 minutes. These organic solutions were trichloroethylene and isopropanol. Etching of the AlGaN semiconductor wafer was done by boiling it in aquaregia for 10 minutes. The sample was then dipped in a HCl:H_2O (1:1) solution for a minute. Between each of these steps the sample was rinsed in deionised water. The deposition of the ohmic contacts was done using the electron beam system and that of the Schottky contacts utilising the resistive evaporator system. The ohmic contacts consisted of Ti (150 Å) /Al (2200 Å) /Ni (400 Å) /Au (500 Å) and the Schottky contact Ni (50 Å)/ Au (50 Å). The annealing was performed isochronously under Ar ambient at the following temperatures: 200 ^{o}C, 300 ^{o}C, 400 ^{o}C, and 500 ^{o}C. The electronic and optical measurements were then done at room temperature.

4.3 RESULTS AND DISCUSSION

The *I*-*V* characteristics of a Ni/Au Schottky photodiode were investigated in this study. Fig. 1 shows the results of the *I*-*V* measurements of the photodiode as deposited and after annealing

at different temperatures. Ni has been used due to the fact that it can adhere well to AlGaN while giving good electrical properties [2]. The effectiveness of thermal annealing can clearly be seen as the reverse leakage current measured at -2 V dropped by 4 orders of magnitude, that is, from 2.07×10^{-9} A for as deposited to 6.97×10^{-13} A for 200 ^{o}C annealing. From there on there was not much difference in terms of the current measured at different annealing temperatures, although it was evident that the reverse current increased after annealing at 500 ^{o}C.

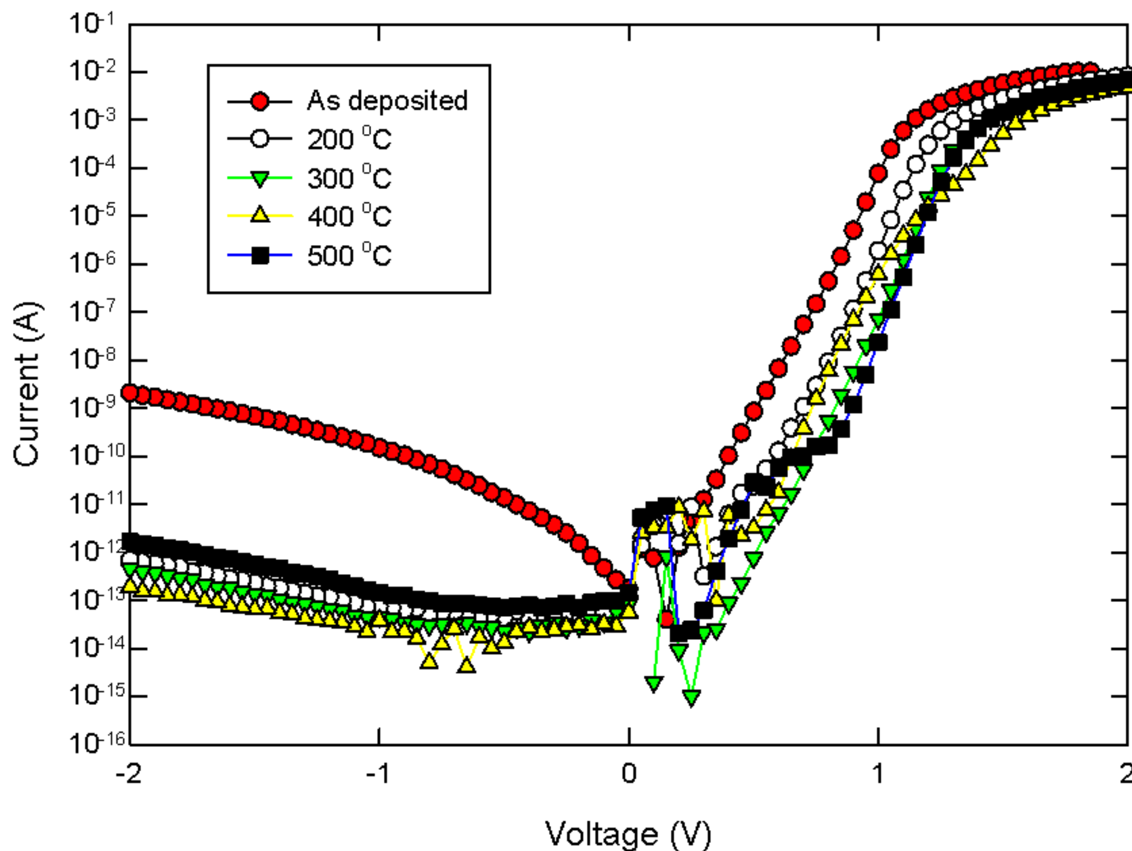

Fig. 1 Current vs. voltage of Ni/Au Schottky diode measured at room temperature after annealing at different temperatures.

The photodiodes showed high noise levels at low voltages. This could be due to the limitation of the measuring equipment as it was measuring at very low currents. In some cases, the reverse current initially decreases from zero bias with increasing reverse bias increasing. This was probably due to deep level defects in the depletion region emptying during the measurement, contributing to the reverse current. The as deposited to 400 ^{o}C annealing temperature graphs have thermionic emission as the dominant current transport mechanism.

At 500 ^{o}C annealing, the diode exhibited signs of a recombination current at low voltages, thermionic emission at intermediate voltages and series resistance dominating at high voltages. As the photodiode was annealed, traps were formed (possibly due to diffusion of impurities into the semiconductor) which led to the generation-combination characteristics observed at low voltages, that is, lower than 1 V [3]. The barrier heights of the diode had an increasing trend with respect to annealing temperatures whereas the ideality factors decreased. As the diode was annealed the barrier height of the photodiode increased from 1.04 eV to 1.46 eV for the as deposited and 500 ^{o}C annealing respectively. The ideality factor decreased from 1.85 to 1.27 for the same temperatures. This shows that the diode improved with annealing temperature as the ideality factor indicates the extent to which the diode is following the ideal diode equation. The extracted electrical values of the photodiode are shown in Table 1.

Table 1 Electrical characteristics obtained for an AlGaN based Ni/Au Schottky photodiode

Annealing temperature	Ideality factor	Barrier height		Reverse current at -2 V (A)
		I-V (eV)	*C-V* (eV)	
As-deposited	1.85	1.04	1.47	2.07×10^{-9}
200 ^{o}C	1.64	1.17	1.59	6.97×10^{-13}
300 ^{o}C	1.64	1.22	1.82	4.54×10^{-13}
400 ^{o}C	1.46	1.25	1.87	1.94×10^{-13}
500 ^{o}C	1.27	1.46	1.89	1.69×10^{-12}

Fig. 2 shows the photocurrent spectrum of a Ni/Au Schottky photodiode measured after annealing at 500 ^{o}C. The photocurrent was generated by radiation in the UV range impinging on the photodiode. This photocurrent reaches a maximum of 4.3×10^{-11} A at 250 nm where the intensity of the light is 3.6×10^{-11} W/cm^2.

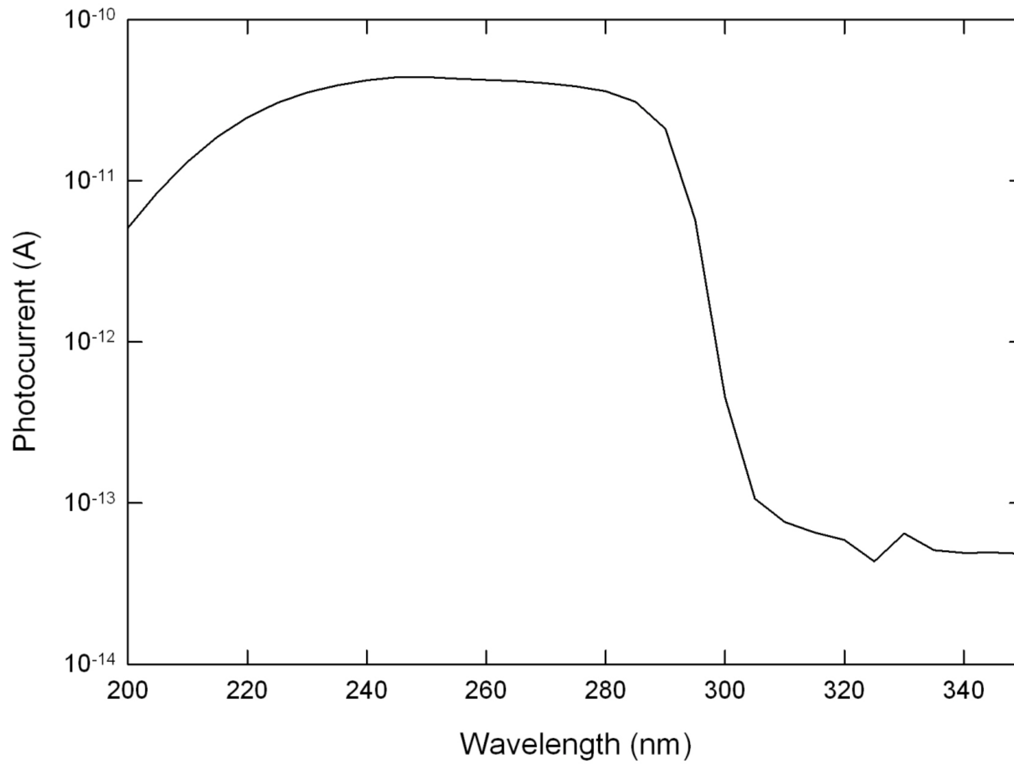

Fig. 2 Photocurrent vs. wavelength of a Ni/Au Schottky photodiode measured at room temperature after annealing at 500 °C

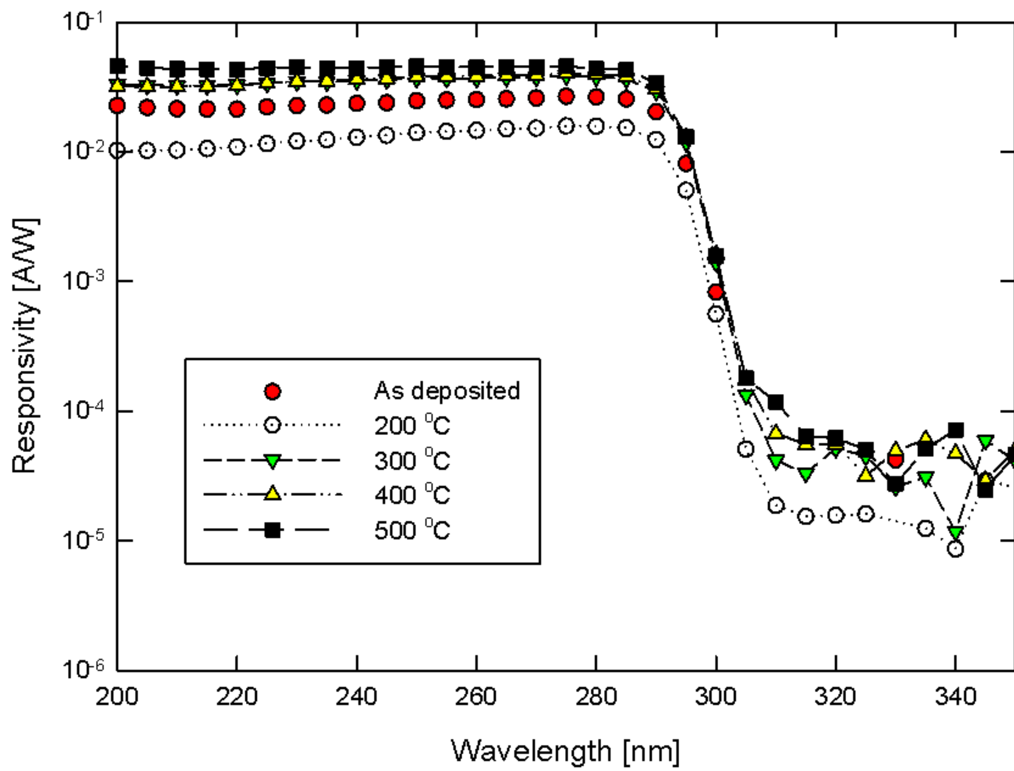

Fig. 3 Responsivity vs. wavelength measured at room temperature after annealing at different temperatures.

The cut-off wavelength for the photodiode was around 292 nm. This corresponds to a bandgap energy of 4.2 eV. In Fig. 3, it can be seen that the value of the UV/visible rejection ratio is approximately 10^3. A responsivity of as high as 46 mA/W at 275 nm was obtained for Ni/Au photodiodes after annealing at 500 ^{o}C. This is comparable to the value obtained by Pau *et al.* [4]. The quantum efficiency vs. wavelength graph of the Schottky diode is given by Fig. 4. The highest quantum efficiency was 28 % which was achieved at 200 nm. This implies that the highest number of electron-hole pairs per incident photon was generated at this wavelength.

Fig. 5 shows the transmittance of a Ni/Au metal layer. The transmittance of incident light is relatively constant for as deposited to 400 ^{o}C annealing where it varies between 43 and 47 % in the 200 to 350 nm wavelength range. As the sample is annealed to 500 ^{o}C, the transmittance of the incident light is no longer constant throughout the abovementioned wavelength range. In the 200 to 300 nm wavelength range, it varies between 50 and 53 %. Between the 300 and 350 nm range the transmittance increases rapidly from 51 to 68 %. This shows that annealing at high temperatures under an Ar gas ambient improves the transmittance of the Ni/Au contact especially the transmittance measured at longer wavelengths. The implication of this occurrence is that a much greater amount of UV radiation will reach the metal semiconductor interface. The increase in transmittance can be partially related to the increase in the responsivity of the diode although other factors such as the intrinsic electrical properties of the photodiode itself have to be considered.

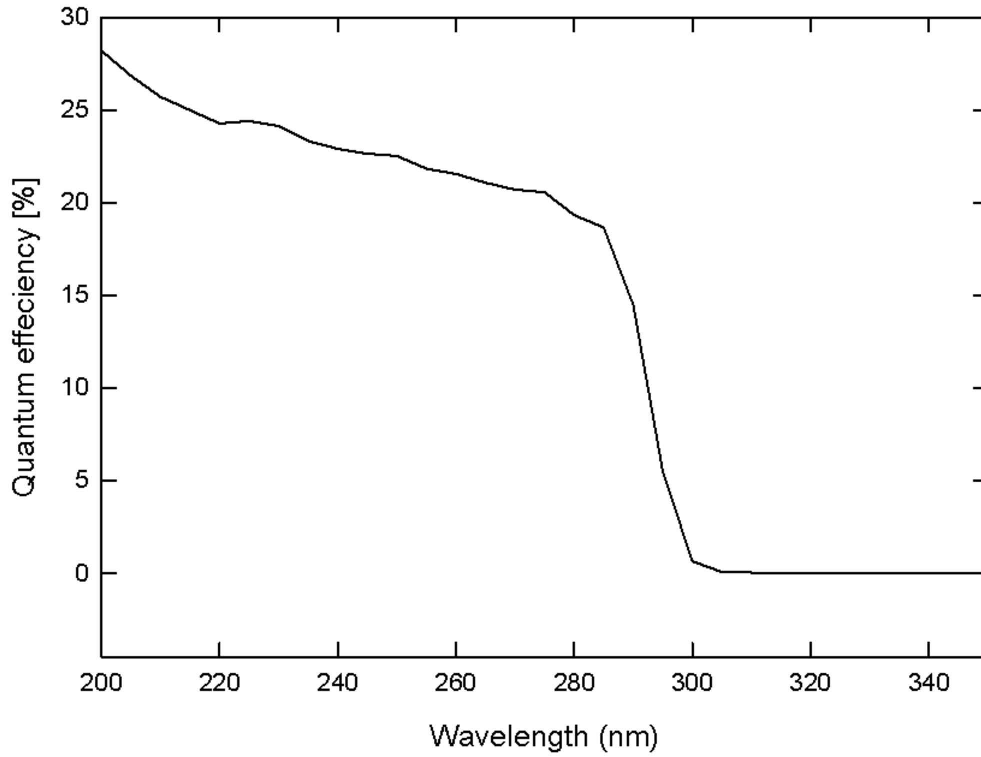

Fig. 4 Internal quantum efficiency spectrum of a Ni/Au Schottky photodiode measured at room temperature after annealing at 500 ^{o}C.

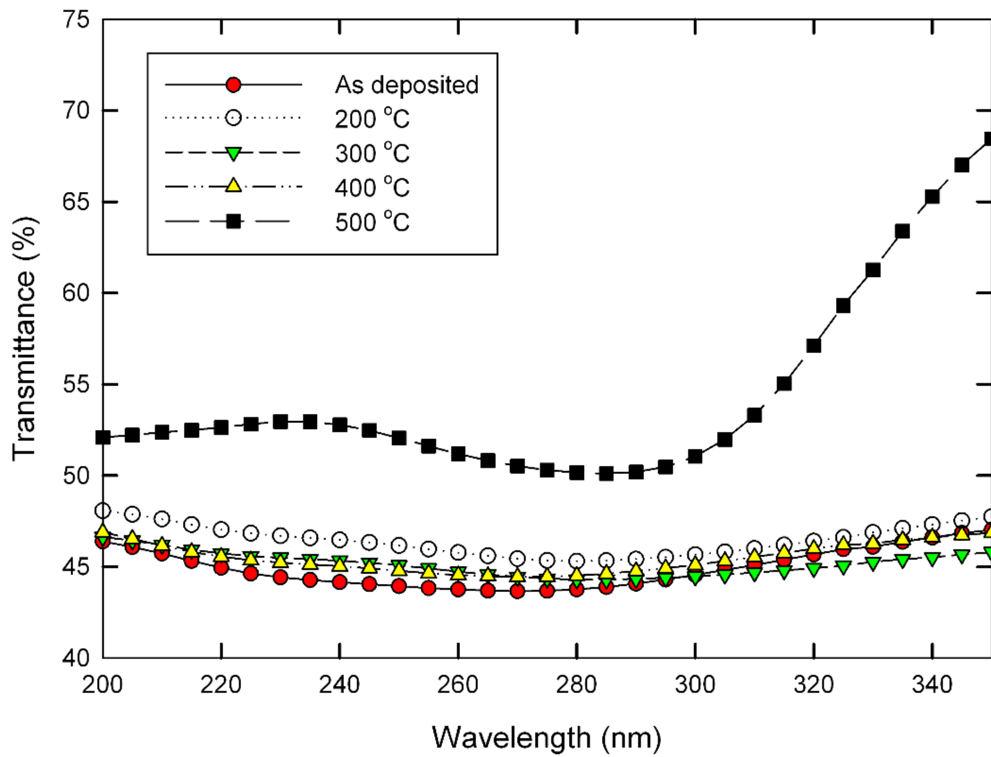

Fig. 5 Transmittance vs. wavelength of a Ni/Au metal layer measured after annealing at different temperatures.

4.4 CONCLUSION

A Ni/Au Schottky photodiode was annealed at different temperatures. It was found that the barrier height was enhanced with increasing annealing temperature. The 500 ^{o}C annealing temperature produced the diode with the highest Schottky barrier height. The values of the diodes increase from 1.04 to 1.46 eV for *I*-*V* measurements and from 1.47 to 1.89 eV for *C*-*V* measurements. It is suspected though that the Schottky barrier height of the *C*-*V* measurement might be a bit too high due to the non uniform doping that has been characteristic of the AlGaN wafers that have been used for this study. Ideality factors for these measurements have decreased with increasing annealing temperature. The peak responsivity value of 46 mA/W was found to be comparable to what has been previously been found for a similar photodiode. The transmittance of the Ni/Au metal layer was relatively constant ranging between 43 and 47 % for the as deposited diode up to 400 ^{o}C annealing temperature. This transmittance, however, varied considerably between 51 to 68 % transmittance after 500 ^{o}C annealing. This shows that annealing the photodiode under Ar ambient improves its electrical and optical properties.

REFERENCES

[1] M. Diale, F.D. Auret, N.G. van der Berg, R.Q. Odendaal, and W.D. Roos, Appl. Surf. Sci. **246**, (2005) 279.

[2] S. Arulkumaran, T. Egawa, H. Ishikawa, M. Umeno, and T. Jimbo, IEEE T. Electron. Dev., **48** (3), (2001) 573.

[3] S.M. Sze, Physics of Semiconductor Devices, John Wiley and Sons, New York, 1981.

[4] J.L. Pau, E. Monroy, E. Muñoz, F.B. Naranjo, F. Calle, M.A. Sánchez-García, E. Calleja, J. Cryst. Growth, **230**, (2001) 544.

UNIVERSITEIT VAN PRETORIA
UNIVERSITY OF PRETORIA
YUNIBESITHI YA PRETORIA

PUBLICATION

Physica B 407 (2012) 1628–1630

Contents lists available at SciVerse ScienceDirect

Physica B

journal homepage: www.elsevier.com/locate/physb

Optoelectronic characterization of Au/Ni/n-AlGaN photodiodes after annealing at different temperatures

P.N.M. Ngoepe *, W.E. Meyer, M. Diale, F.D. Auret, L. van Schalkwyk

Department of Physics, University of Pretoria, Pretoria 0002, South Africa

ARTICLE INFO

Available online 25 September 2011

Keywords:
Annealing
Schottky photodiode
AlGaN

ABSTRACT

The optoelectronic characteristics of Ni/Au Schottky photodiodes based on $Al_{0.35}Ga_{0.65}N$ were investigated. The transmission of the Ni (50 Å)/Au (50 Å) layer was determined by evaporating it on a quartz substrate. As evaporated, the transmission coefficient in the 200–350 nm wavelength range was found to be 43 to 48%. Annealing at temperatures of up to 400 °C did not influence the transmission coefficient. After annealing at 500 °C, the transmission coefficient increased from 50 to 68% over the 200–350 nm range. The reverse bias current was optimised in terms of annealing temperature and was found to be as low as 1.94×10^{-13} A after annealing at 400 °C for a 0.6 mm diameter contact. The Schottky barrier heights increased with annealing temperature reaching as high as 1.46 and 1.89 eV for *I–V* and *C–V* measurements, respectively. The quantum efficiency was measured to be 20.5% and the responsivity reached its peak of 0.046 A/W at 275 nm. The cut-off wavelength was 292 nm.

© 2011 Elsevier B.V. All rights reserved.

1. Introduction

Wide bandgap materials have been of interest recently because of their suitability for use in industrial, scientific and military applications. Aluminium gallium nitride ($Al_xGa_{1-x}N$) is such a material and has attracted a lot of attention for ultraviolet (UV) detection [1–4]. This is because $Al_xGa_{1-x}N$ based photodiodes have an adjustable cut-off wavelength, which can be varied by changing the Al composition. Another contributing factor is that AlGaN is a direct bandgap semiconductor. For the right choice of Al mole fraction, these detectors are intrinsically solar blind, thus eliminating the need for filters and thereby decreasing the size and cost of the complete system. The applications of UV sensitive photodetectors include missile plume sensing, flame detection and chemical sensing. For front illuminated diodes, a transparent/semi-transparent non reflective Schottky contact needs to be produced. This can be done by a number of methods such as depositing a very thin Schottky layer and/or annealing the diode under different conducive conditions to form a transparent conductive metal layer. Careful steps must be taken however to ensure that the transparency is achieved without degrading the electrical characteristics of the diode. The properties of Ni/Au have been investigated for different applications and by various methods. Miaru et al. investigated thermal annealing effects on Ni/Au and found them to be quite small [5]. Chang et al. also performed thermal annealing studies for Ni/Au contacts on AlGaN for MSM photodiodes [6]. In this paper we endeavour to study the thermal annealing effects of a Ni/Au on $Al_{0.35}Ga_{0.65}N$ Schottky contact by investigating the optical and electronic characteristics after annealing at different temperatures in Ar gas.

2. Experimental

The AlGaN sample used in this study was grown by hydride vapour phase epitaxy (HVPE) at Technologies and Devices International, Inc. (TDI). The structure of the sample, as per specification from TDI, is as follows (from the top layer): 0.7 μm $Al_{0.35}Ga_{0.65}N$, 0.2 μm Si doped $Al_{0.35}Ga_{0.65}N$, 1.2 μm Si doped GaN, 0.8 μm undoped GaN and a sapphire substrate (polished on one side). For the cleaning process, the AlGaN wafer was degreased in trichloroethylene and in isopropanol, respectively, for 3 min. It was then etched in boiling aqua regia for 10 min and dipped in HCl:H_2O (1:1) for a minute. In between all the chemical cleaning processes, de-ionised water was used to rinse the chemicals from the sample. The sample was then blow-dried with N_2. Ti (150 Å)/Al (2200 Å)/Ni (400 Å)/Au (500 Å) layers were deposited as an ohmic contact onto the AlGaN wafer by means of electron beam deposition. Subsequent to this, a Ni (50 Å)/Au (50 Å) Schottky contact was deposited using a resistive evaporation system. These metals were deposited without annealing the ohmic contacts. The Schottky contact mask produced Schottky diodes with a diameter of 0.6 mm. *I–V* measurements were performed using an HP 4140B pA Metre/DC Voltage Source.

* Corresponding author. Tel.: +27 12 420 3508; fax: +27 12 362 5288.
E-mail address: phuti.ngoepe@up.ac.za (P.N.M. Ngoepe).

0921-4526/$ - see front matter © 2011 Elsevier B.V. All rights reserved.
doi:10.1016/j.physb.2011.09.102

UNIVERSITEIT VAN PRETORIA
UNIVERSITY OF PRETORIA
YUNIBESITHI YA PRETORIA

C–V measurements were done using an HP 4192 A LF Impedance Analyser. The theory used for determining the I–V and C–V characteristics is well known [7,8]. For photo measurements, a Digikrom DK 240 1/4 m monochromator and a 30 W deuterium lamp were used. The light intensity was calibrated with a Si-based detector. Due to the nature of our sample, the measurements were performed by means of front illumination. There are a few parameters, which are important to the optical characterization of photodiodes. Two of these have been measured for our study namely the quantum efficiency and the responsivity. The sample was isochronously annealed in a furnace at different ambient temperatures for 5 min at 200, 300, 400 and 500 °C in argon gas. After each annealing step, opto-electronic characterization was done at room temperature (about 300 K). In order to perform transmittance measurements, a Ni (50 Å) /Au (50 Å) metal combination was deposited on a quartz substrate. This sample was annealed under the same conditions as the AlGaN sample. Transmission measurements were done using a Perkin Elmer Lambda 25 UV/VIS Spectrometer.

3. Results and discussion

Fig. 1 gives the reverse current of the Schottky photodiode measured after annealing at different temperatures. Up to 400 °C, the reverse current at −2 V decreased with increasing annealing temperature. At this voltage, the reverse current decreased by 3 orders of magnitude from 2.07×10^{-9} to 6.97×10^{-13} A (as-deposited to 200 °C annealing). The reason for this could be that annealing the sample caused metal alloys to form. It has also been suggested by Kim et al. [9] that annealing Schottky diodes causes a reduction in the interface state densities. These interface states can hamper electrical conductivity in the forward direction and increase leakage current in the reverse direction. Annealing at 500 °C caused the reverse current at −2 V bias to increase by one order of magnitude. The reason for this increase could be due to Au diffusing through the Ni to the metal–semiconductor interface [5] as the diode starts to degrade. It can also be seen that for the graphs of annealing temperatures 200–500 °C, the reverse leakage current initially decreased with an increase in applied reverse bias voltage. This is a measurement artefact due to traps emptying during the measurement.

The forward bias characteristics are shown in Fig. 2. We observed an improvement in terms of the barrier height with increasing annealing temperature. For the I–V characteristics the barrier height increased from 1.038 eV (as-deposited) to 1.457 eV (500 °C). That of the C–V measurements increased from 1.456 eV (as-deposited) to 1.895 eV (500 °C). The C–V barrier heights are unusually high. This might be due to the assumption that the carrier density is constant right up to the interface, which might not be the case with these diodes. The ideality factor of the diodes improved with annealing temperatures from a value of 1.85–1.27 as shown in Table 1. Fig. 2 shows the forward bias I–V characteristics. The initial data points have been removed. This noise could be caused by the fact that we were measuring at low currents and the equipment was reaching its limit. The I–V characteristics of all the diodes were explained well by the thermionic emission model. The I–V characteristics of the as-deposited and 300 °C annealed samples were dominated by thermionic emission and series resistance. The samples annealed at 200 °C and 500 °C included the aforementioned current transport mechanism as well as generation recombination, although in the sample annealed at 500 °C it was more significant. The 400 °C annealed sample had all the aforementioned mechanisms and included a high injection region.

The transmittance spectrum of Ni/Au (Fig. 3) indicates that the transmittance does not change much from that of the as-deposited material up to an annealing temperature of 400 °C. The transmittance ranges from 43 to 49% within the 200 to 400 nm wavelength range. It is only at 500 °C annealing that the transmittance increased significantly. The transmittance measured after annealing at this temperature ranged from 50 to 74% within the same wavelength range indicating that the Ni/Au became more transparent to UV light. The responsivity of the photodiode after annealing at different temperatures is shown in Fig. 4. It decreased from as-deposited to annealing at 200 °C and then increased with each subsequent annealing step. The responsivity

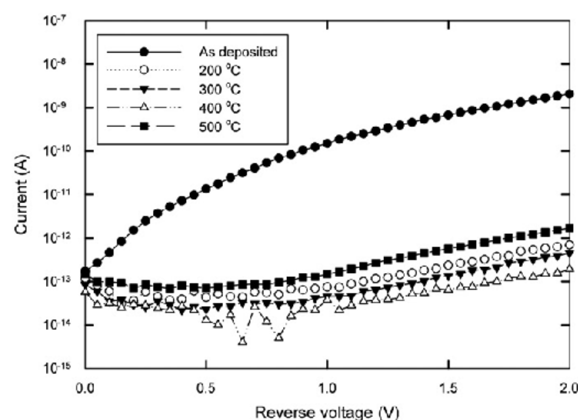

Fig. 1. Reverse bias I–V characteristics of Ni/Au on AlGaN after different annealing temperatures.

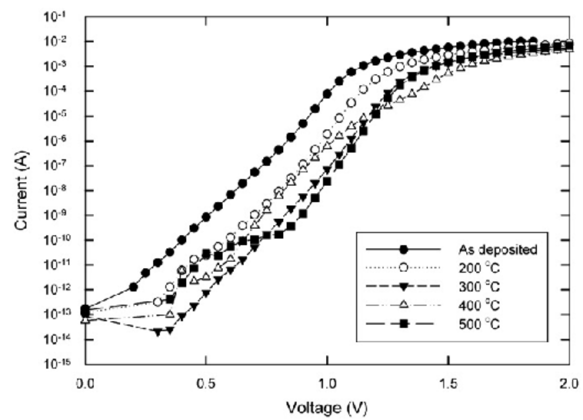

Fig. 2. Forward bias I–V characteristics of Ni/Au on AlGaN after different annealing temperatures.

Table 1
Electrical properties of Ni/Au on AlGaN Schottky photodiodes.

Annealing temperature	Ideality factor	Barrier height		Reverse current at −2 V (A)
		I–V (eV)	C–V (eV)	
As-deposited	1.85	1.04	1.47	2.07E−09
200 °C	1.64	1.17	1.59	6.97E−13
300 °C	1.64	1.22	1.82	4.54E−13
400 °C	1.46	1.25	1.87	1.94E−13
500 °C	1.27	1.46	1.89	1.69E−12

UNIVERSITEIT VAN PRETORIA
UNIVERSITY OF PRETORIA
YUNIBESITHI YA PRETORIA

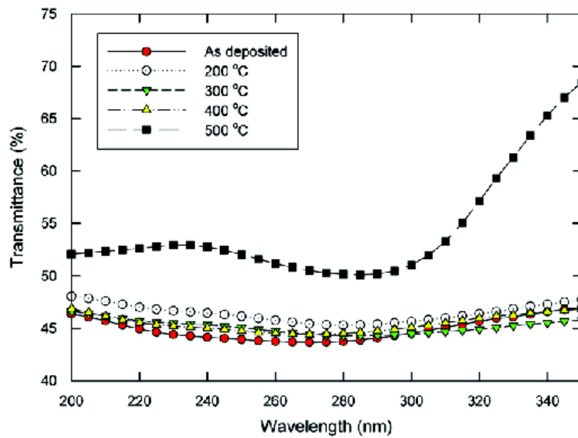

Fig. 3. Transmittance spectrum of Ni/Au deposited on a quartz substrate.

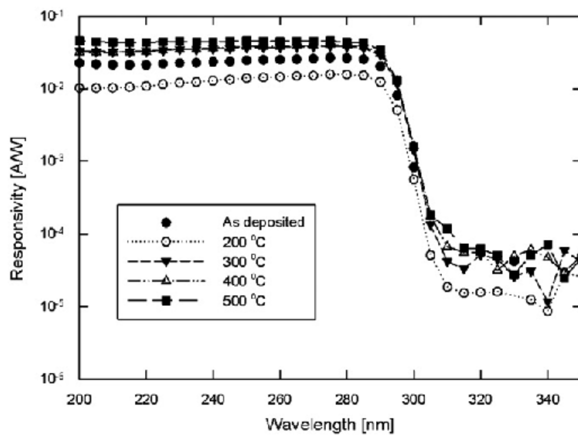

Fig. 4. Spectral responsivity of Ni/Au Schottky photodiode on AlGaN at different temperatures.

showed its highest value at 500 °C annealing temperature. This also corresponded to the transmittance shown in Fig. 3. At 500 °C annealing temperature the Ni/Au contact exhibited its highest transmittance. The range of the responsivity of the photodiode is from 200 nm to about 300 nm, where a sharp cut-off wavelength occurred at 292 nm. Theoretically, the cut-off wavelength can be determined from the ideal diode equation when the bandgap is known. In our case, the bandgap of $Al_{0.35}Ga_{0.65}N$ was found by interpolation between AlN and GaN. It has been calculated by Omnes et al. [10] using photothermal deflection spectroscopy (PDS). The value for this has been measured as 4.22 eV, which corresponds to a cut-off wavelength of around 294 nm. This has been confirmed by Monroy et al. [11]. The peak responsivity at zero bias voltage for the different annealing temperatures occurred at a wavelength of 275 nm. Fig. 5 shows the values

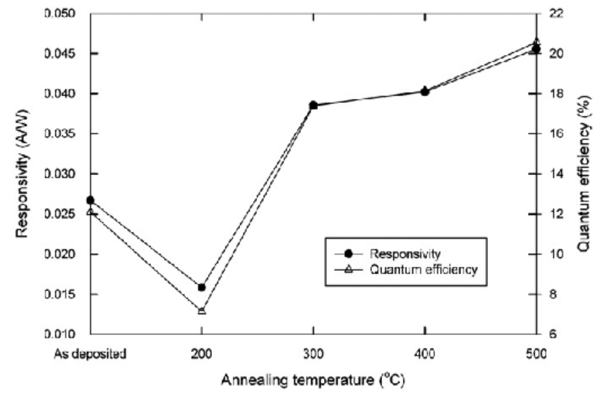

Fig. 5. Responsivity and quantum efficiency as a function of annealing temperature of a Ni/Au on AlGaN Schottky photodiode.

extracted for the responsivity and quantum efficiency after annealing at different temperatures. The trend of the responsivity and the quantum efficiency are similar. The maximum responsivity and quantum efficiency have been measured as 0.046 A/W and 20.5%, respectively.

4. Conclusion

Ni/Au Schottky photodiodes based on $Al_{0.35}Ga_{0.65}N$ have been successfully fabricated and characterized. The annealing temperature has been optimised and the lowest reverse current was found to be after annealing at 400 °C. The photodiode was found to be responsive in a specific wavelength range (200–300 nm). The peak responsivity was measured as 0.046 A/W and a quantum efficiency of as high as 20% at 275 nm wavelength. The transmittance spectrum showed that Ni/Au deposited on quartz has a significantly higher transmittance after annealing at 500 °C.

References

[1] E. Munoz, E. Monroy, J.L. Pau, F. Calle, F. Omnes, P. Gibart, J. Phys.: Condens. Matter 13 (2001) 7115.
[2] K.Y. Park, B.J. Kwon, J.H. Son, Y.H. Cho, Phys. Status Solidi C 3 (6) (2006) 2299.
[3] E. Monroy, F. Omnes, F. Calle, Semicond. Sci. Technol. 18 (2003) R33.
[4] M. Razeghi, Proc. of the IEEE 90 (6) (2002) 1006.
[5] N. Miaru, T. Nanjo, M. Suita, T. Oishi, Y. Abe, Ozeki, H. Ishikawa, T. Egawa, T. Jimbo, Solid-State Electron. 48 (2004) 689.
[6] P.C. Chang, C.H. Chen, S.J. Chang, Y.K. Su, C.L. Yu, P.C. Chen, C.H. Wang, Semicond. Sci. Technol. 19 (2004) 1354.
[7] D.K. Schroeder, Semiconductor Materials and Device Characterization, John Wiley and Sons, New York, 1998.
[8] S.M. Sze, Physics of Semiconductor Devices, 2nd ed., John Wiley and Sons, New York, 1981.
[9] H. Kim, M.L. Schutte, J. Lee, W. Lu, J.C. Mabon, J. Electron. Mater. 36 (9) (2007) 1149.
[10] F. Omnes, N. Marenco, B. Beaumont, Ph de Mierry, E. Monroy, F. Calle, E. Munoz, J. Appl. Phys. 86 (9) (1999) 5286.
[11] E. Monroy, F. Calle, J.L. Pau, J. Sanchez, E. Munoz, F. Omnes, B. Beaumont, P. Gibart, J. Appl. Phys. 88 (4) (2000) 2081.

CHAPTER 5

RESULTS AND DISCUSSION 2

5.1 INTRODUCTION

A good Schottky contact is one that at least for forward conduction, obeys the thermionic emission equation to a good approximation and has a high Schottky barrier height, low reverse leakage current and low series resistance. In addition, the ability to withstand high temperatures is frequently a requirement. It has been found by Miura *et al.* that the insertion of a metal with a high metal work function between Ni and Au improves the quality of Schottky diodes on GaN [1]. In this chapter a comparison is made with regards to the opto-electrical characteristics of Ni/Au and Ni/Ir/Au Schottky photodiodes measured at room temperature after different annealing temperatures.

5.2 EXPERIMENTAL

The deposition of the metals on the AlGaN wafers was performed using both an e-beam system and a resistive evaporator system. The ohmic contacts were deposited with the e-beam system using the metallisation scheme Ti (150 Å)/ Al (2200 Å)/ Ni (400 Å)/ Au (500 Å). Prior to the deposition of the Schottky contacts the samples were dipped in a HCl:H_2O (1:1) solution in which the HCl content is 17 %. This was done to remove some of the contaminants that might have settled on the wafer. As the ohmic contacts had not been annealed, the samples were dipped for no longer than 10 seconds in the acidic solution. This was to avoid prolonged interaction of the ohmic contacts with the acid as this would begin to dissolve the contact off the semiconductor. Once the final cleaning process had been done, the sample was blow dried in N_2. The Ni (20 Å)/ Ir (30 Å)/ Au (50 Å) Schottky contacts were deposited using the e-beam system. This was due to the fact that Ir has a high melting point and therefore requires a high temperature evaporation system. Another reason was that the e-beam system can take up to four different metals for a single deposition cycle. The Ni (20 Å)/

Au (50 Å) Schottky contacts were deposited using the resistive evaporator system. Both the Ni/Au and Ni/Ir/Au Schottky contacts had diameters of 0.6 mm. Annealing under an Ar ambient was isochronously performed at temperatures 200, 300, 400, and 500 °C for 5 minutes. After each annealing step electrical and optical measurements were performed at 25 °C. The irradiance used for the optical measurements is shown in Fig. 1.

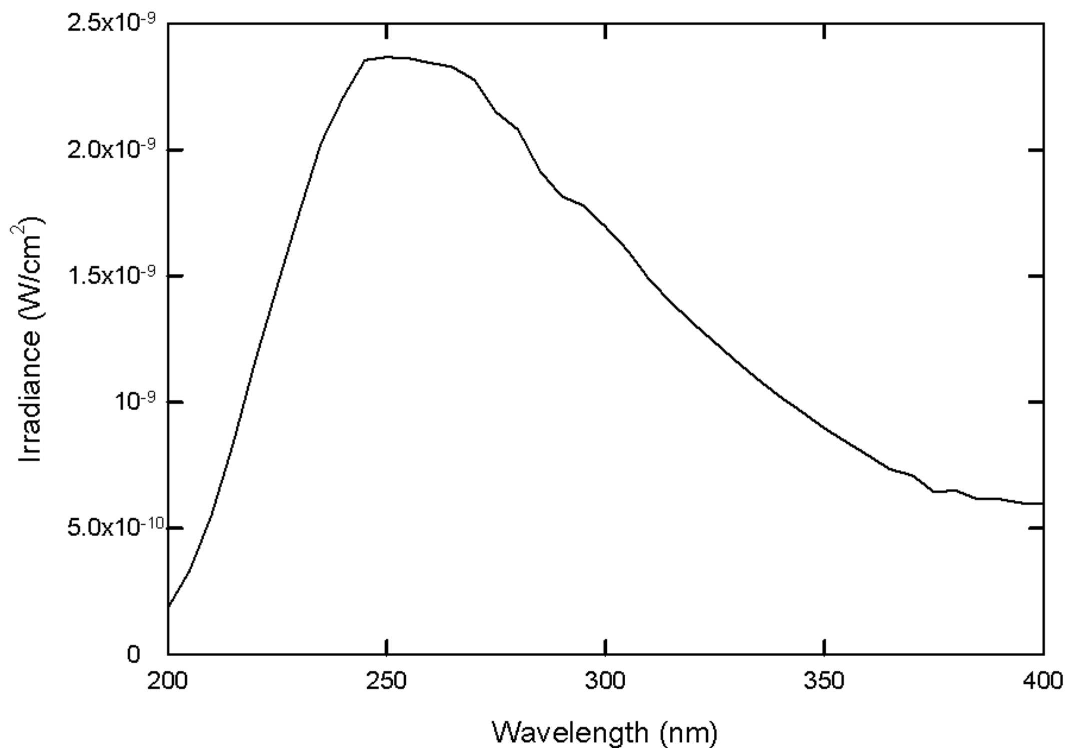

Fig. 1 Irradiance vs. wavelength of a Digikrom monochromator

5.3 RESULTS AND DISCUSSION

5.3.1 Electrical properties

The *I-V* characteristics of the Ni/Au Schottky photodiode after various annealing temperatures are shown in Fig. 2. The heat treatment of the photodiodes at low temperatures improved the reverse bias characteristics. The reverse current of the Ni/Au photodiode measured at -1 V decreased with annealing temperature up to 400 °C. At 500 °C annealing the diode deteriorated and exhibited a higher reverse current. The forward bias characteristics measured after 500 °C annealing had a generation-recombination pattern at lower voltages which is attributed to the introduction of recombination centres [2].

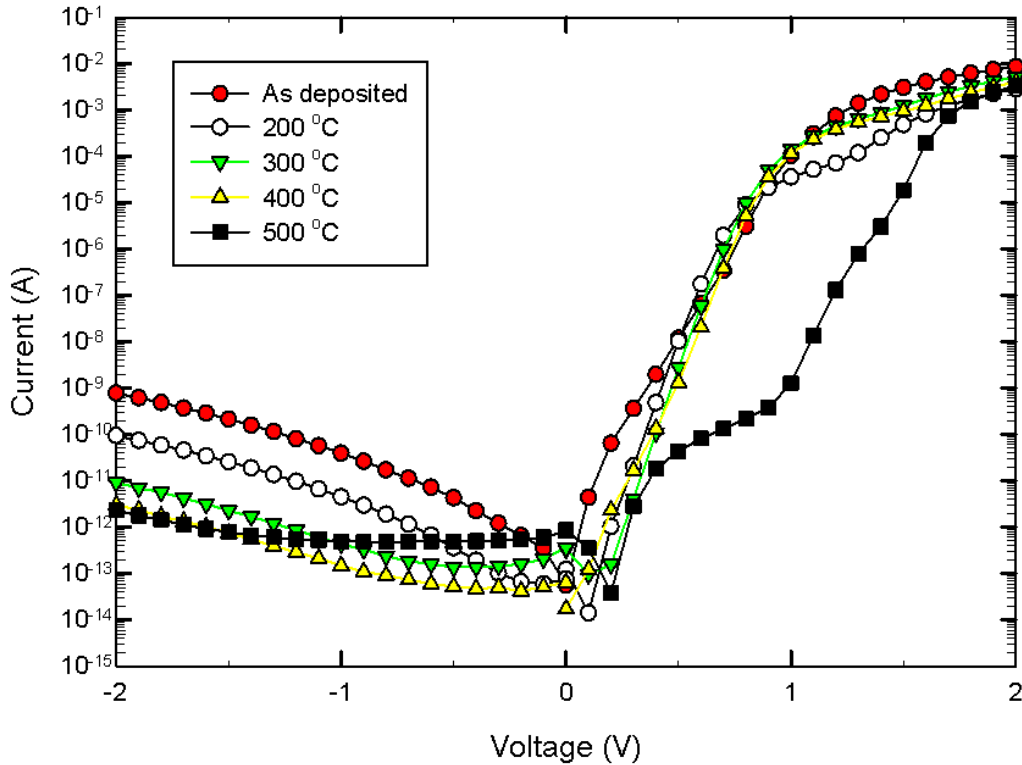

Fig. 2 *I-V* characteristics of Ni/Au Schottky photodiode measured at room temperature after annealing at different temperatures.

After annealing at lower temperatures the current voltage pattern of the Ni/Ir/Au photodiode was similar to that of the Ni/Au photodiode (Fig. 2) as can be seen in Fig. 3. The reverse current of both photodiodes at -1 V decreases with increasing annealing temperature. In contrast to the Ni/Au Schottky photodiode, the reverse current characteristics of the Ni/Ir/Au Schottky photodiode continued to improve up to 500 ^{o}C annealing. This could be attributed to the Ir layer which prevented diffusion of Au through the Ni layer. Iridium is a metal that has a higher thermal stability than Ni and Au. It also has a greater density than both metals. The indiffusion of Au and Ni has been known to cause deterioration of devices. This degradation has also been attributed to the formation of metal gallides and/or nitrides [3]. The initial decrease in the reverse current with increasing reverse bias was probably due to deep level defects emptying. In both the Ni/Au and the Ni/Ir/Au photodiode, the series resistance of the contacts increased with annealing temperature.

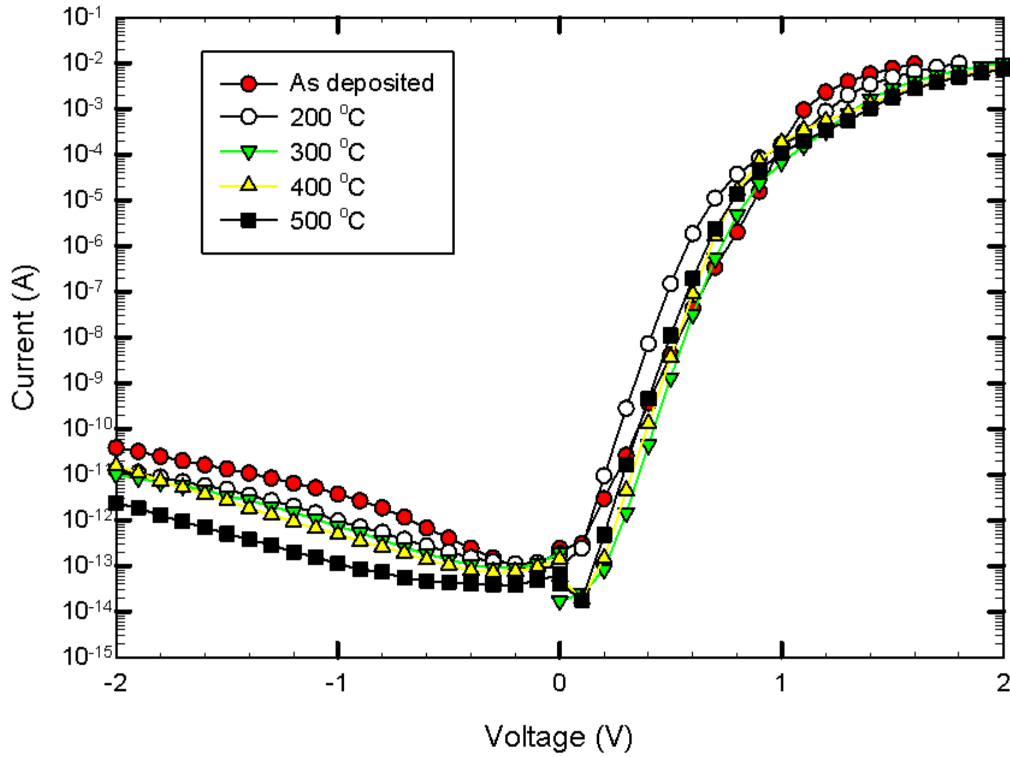

Fig. 3 *I-V* characteristics of Ni/Ir/Au Schottky photodiode measured at room temperature after annealing at different temperatures

Table 1 gives the electrical properties of Ni/Au and Ni/Ir/Au Schottky photodiodes measured as deposited and after annealing at 500 °C. The Schottky barrier height of both the Ni/Au and Ni/Ir/Au Schottky photodiodes improved with increasing annealing temperature. The Ni/Au photodiode barrier height increased from 0.91 to 1.26 eV whilst that of Ni/Ir/Au photodiode showed a smaller increase from 1.01 to 1.10 eV. The ideality factors of the diodes decreased from 2.18 to 1.90 for the Ni/Au photodiode and from 1.75 to 1.22 for the Ni/Ir/Au photodiode. The values for the barrier heights of the Ni/Au Schottky photodiode are comparable with what has been found in literature. A value of as high as 1.37 eV has been determined by Lu *et al.* [4]. The same could be said about the Ni/Ir/Au diode where a diode with a Schottky barrier height of 1.05 eV was found [1].

Table 1 The electrical properties of Ni/Au and Ni/Ir/Au Schottky photodiodes measured after different annealing temperatures.

Schottky metals	Annealing temperature	Schottky barrier height (eV)	Ideality factor	Saturation current (A)	Series resistance (ohm)	Reverse current at -1 V (A)
Ni/Au	As deposited	0.91	2.18	1.51×10^{-12}	85	3.95×10^{-11}
	500 ^{o}C	1.26	1.90	1.63×10^{-18}	88	4.94×10^{-13}
Ni/Ir/Au	As deposited	1.01	1.75	4.15×10^{-14}	47	3.73×10^{-12}
	500 ^{o}C	1.10	1.22	9.31×10^{-16}	82	1.12×10^{-13}

5.3.2 Responsivity

Fig. 4 shows a comparison between the responsivity of the Ni/Au and the Ni/Ir/Au Schottky photodiode. This responsivity was measured at zero bias. The Ni/Au Schottky photodiode had the highest responsivity. As can be seen from the abovementioned figure, the cut-off responsivity was 292 nm for both photodiodes. This is because the cutoff wavelength is related to the bandgap energy of the semiconductor which for $Al_{0.35}Ga_{0.65}N$ is 4.22 eV [5]. The Ni/Au photodiode has a peak responsivity of 77 mA/W at 200 nm whereas the Ni/Ir/Au has 25 mA/W at 275 nm. The higher responsivity of the Ni/Au is partly attributed to the thickness of the metal layers. The combined Ni/Au layer was thinner than the Ni/Ir/Au layer thus causing more radiation to reach the metal-semiconductor interface. This caused the responsivity of the Ni/Au device to be greater. The photocurrent to reverse current ratios reached as high as 10^2.

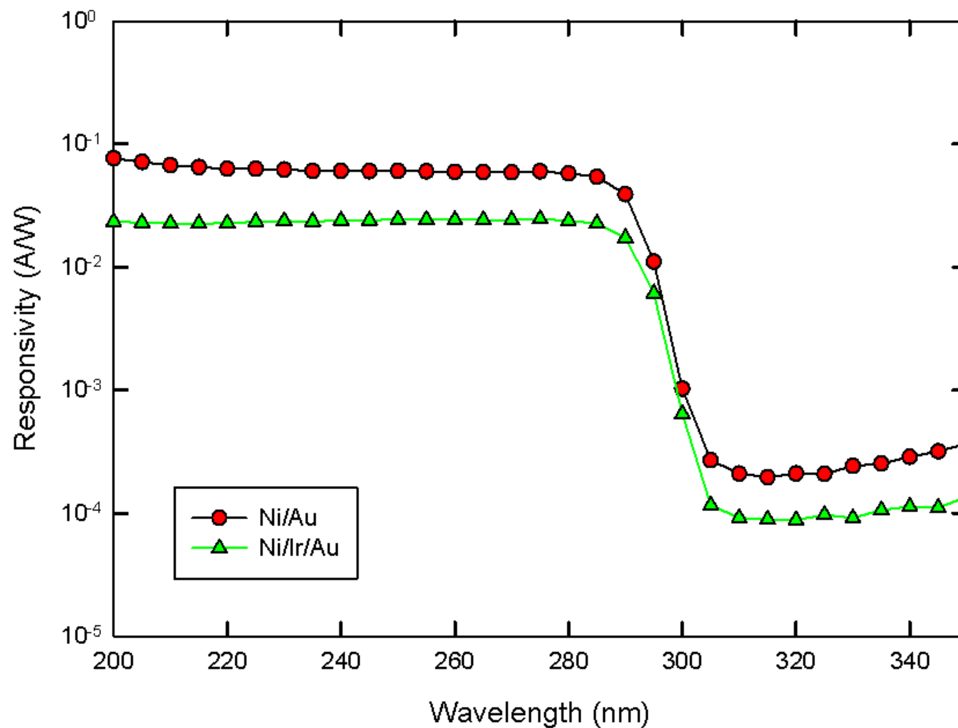

Fig. 4 The responsivity vs. the wavelength of a Ni/Au and Ni/Ir/Au Schottky photodiode

5.3.3 Current voltage measurements under different illumination wavelengths

The trends of the current voltage characteristics of the Ni/Au and Ni/Ir/Au Schottky photodiodes as shown by Figs. 5 to 8 were similar. The photocurrent was dominant at the lower bias voltages of the Schottky photodiodes. In the as deposited Schottky photodiodes the photocurrent dominated up to -1 V whereas after 500 ^{o}C annealing, the photocurrent dominated up to -3 V. The photocurrent to reverse current ratios for both these samples reached as high as 10^2 depending on the voltage applied. The photocurrent was generated by the electrons that flow from the metal into the semiconductor, and remained essentially constant irrespective of the applied bias. At higher reverse bias voltage, the photo-generated current was dominated by the reverse leakage current of the diode. In some cases the un-illuminated diode showed a higher leakage current at 0 V which was probably due to deep level traps emptying. From these graphs it is clear that the peak of the responsivity was 275 nm as both the responsivity at 210 nm and the cut-off wavelength (292 nm) were lower.

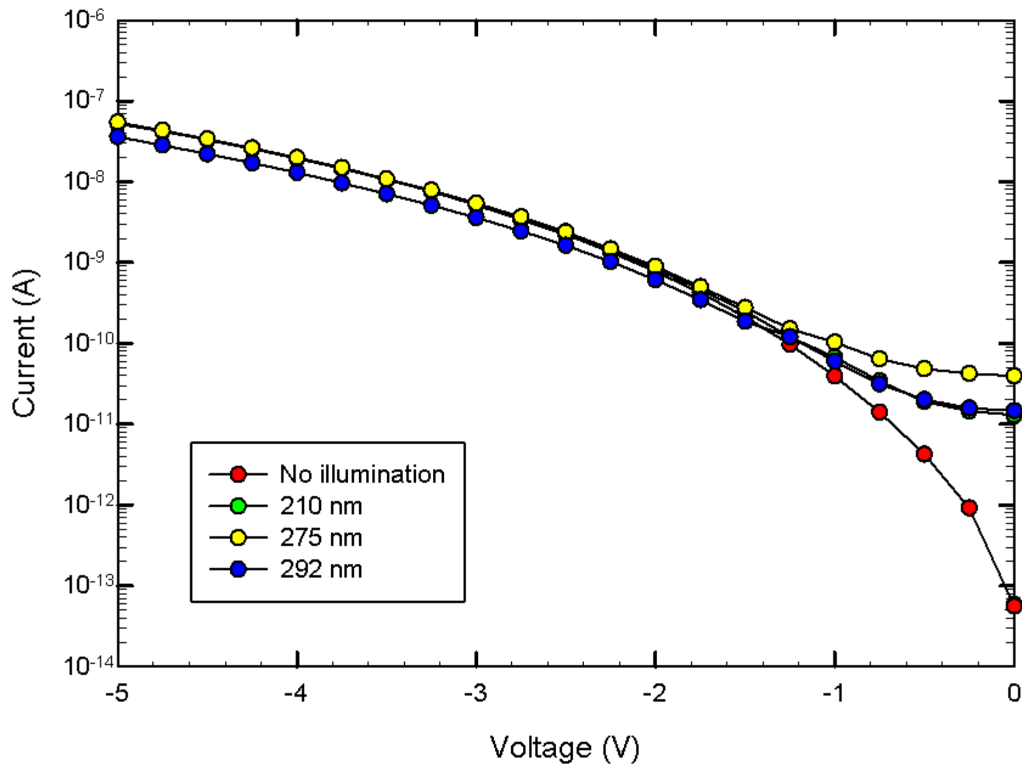

Fig. 5 Reverse current vs. voltage characteristics of an as deposited Ni/Au Schottky photodiode measured at room temperature under different illumination wavelengths.

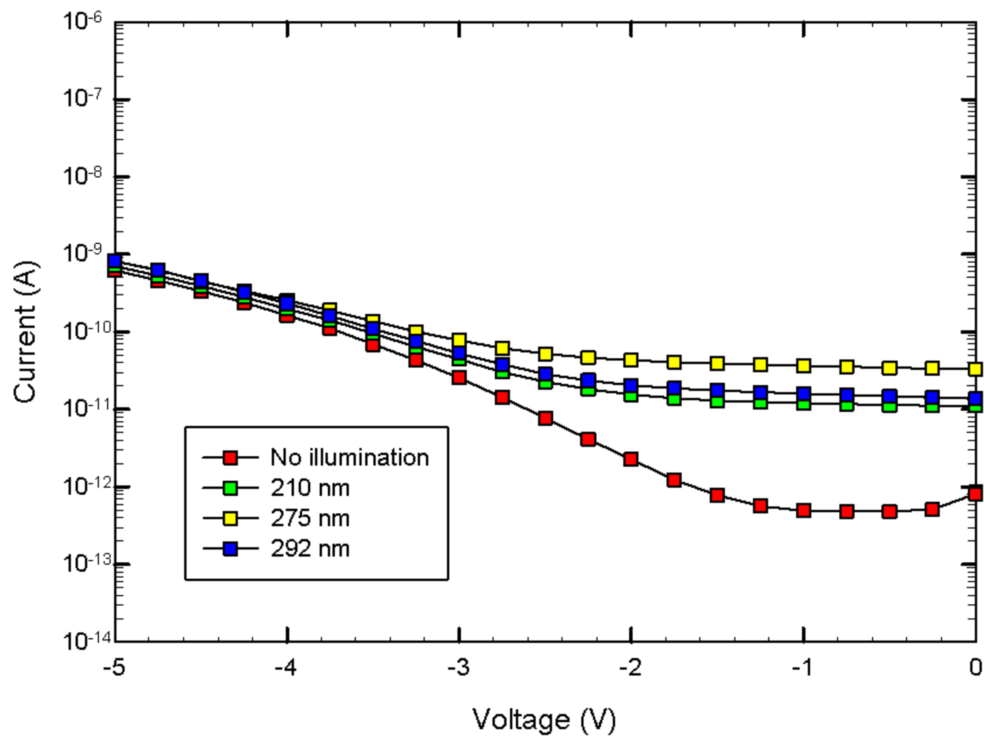

Fig. 6 Reverse current vs. voltage characteristics of a 500 °C annealed Ni/Au Schottky photodiode measured at room temperature under different illumination wavelengths.

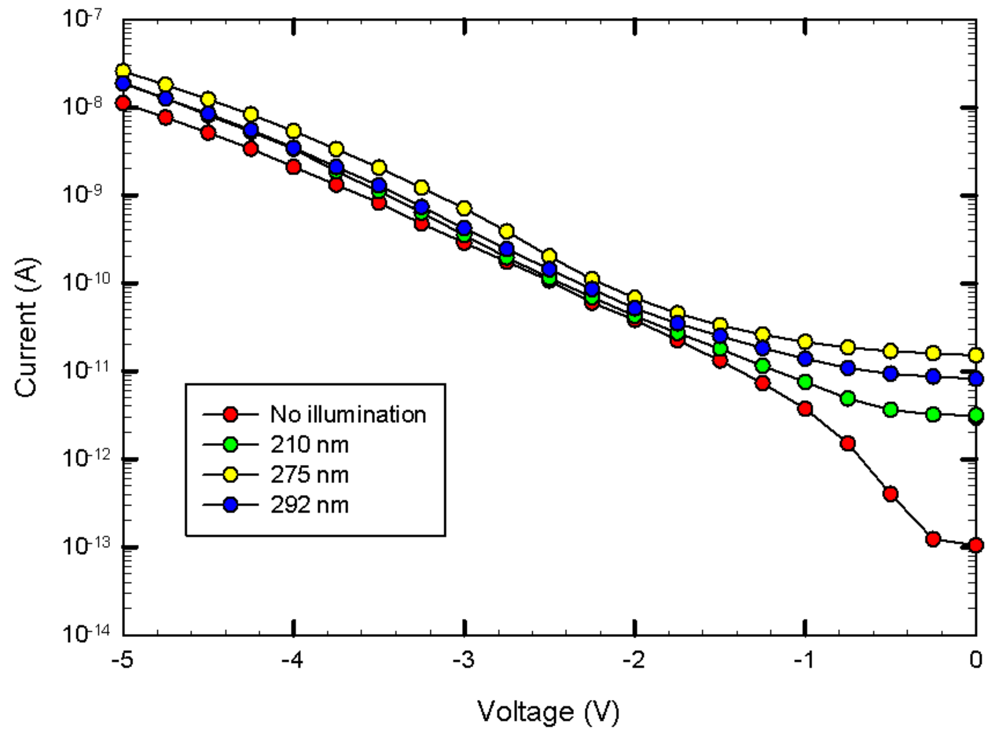

Fig. 7 Reverse current vs. voltage characteristics of an as deposited Ni/Ir/Au Schottky photodiode measured at room temperature under different illumination wavelengths.

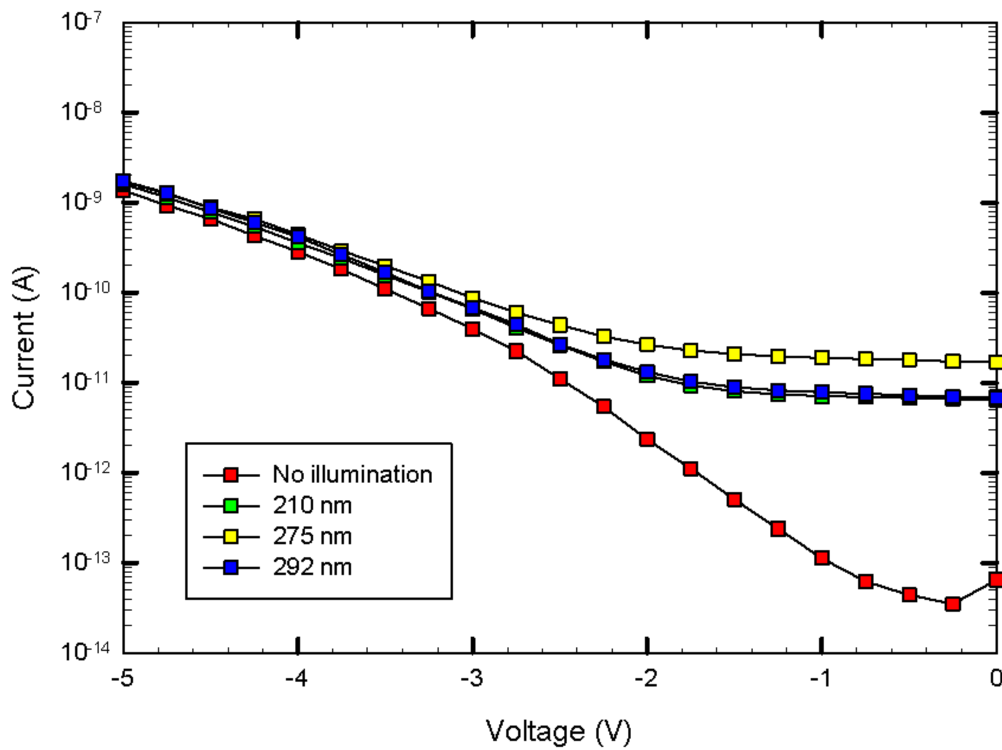

Fig. 8 Reverse current vs. voltage characteristics of a 500 ^{o}C annealed Ni/Ir/Au Schottky photodiode measured at room temperature under different illumination wavelengths

5.3.4 Transmission

The transmittance of the Ni (20 Å)/ Au (50 Å) layer was higher than that of the Ni (20 Å)/ Ir (30 Å)/ Au (50 Å) layer due to the fact that the thicknesses of the latter was greater. Fig. 9 shows transmittance of the Ni/Au layer in the wavelength range 200 to 360 nm measured after annealing at different temperatures. After annealing at low temperatures, the transmittance was lower and constant throughout the entire wavelength range. As the annealing temperature increased, the transmittance also increased. After annealing at 500 ^{o}C the transmission reached a peak of 85 % at a wavelength of 360 nm. In contrast to the Ni/Au layer, the Ni/Ir/Au layer at lower temperatures did not exhibit a constant transmittance over a wide wavelength range as depicted in Fig. 10. At lower annealing temperatures, focusing on the 200 to 280 nm wavelength range, the transmittance decreased with increasing wavelength, but remained relatively constant from 280 to 360 nm. The transmittance of the Ni/Ir/Au layer after annealing at 400 ^{o}C and 500 ^{o}C had the same trend. They had a 'u-shaped' figure in the 200 to 360 nm wavelength range. After 500 ^{o}C annealing the transmittance of the metal layer decreased. It was lower than the transmittance measured after 400 ^{o}C annealing. In the intermediate region, the 500 ^{o}C has lower values of transmittance than those of the 300 ^{o}C spectrum. It therefore indicated that the best temperature for annealing the Ni/Ir/Au metal layer was 400 ^{o}C.

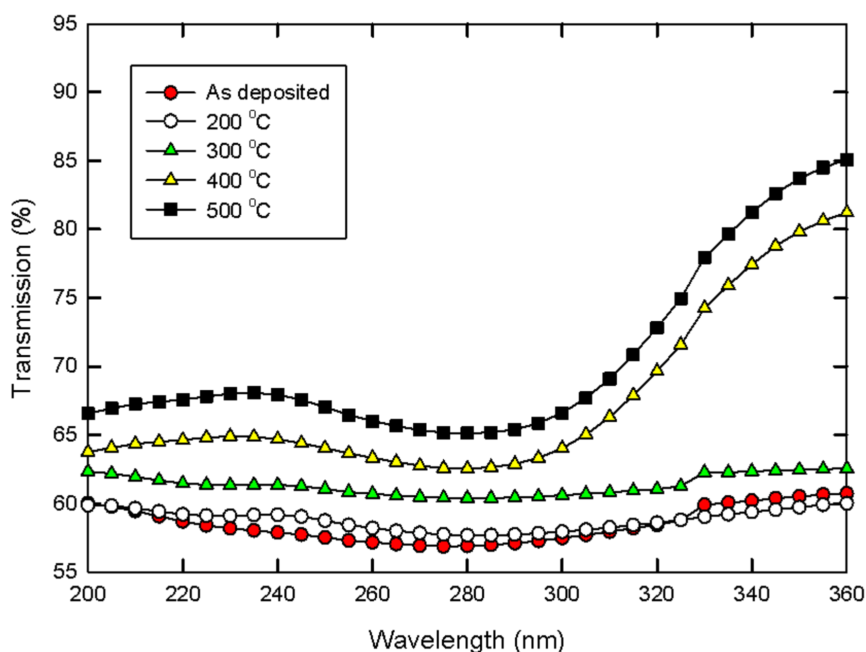

Fig. 9 Transmission vs. wavelength of a Ni/Au metal layer deposited on a quartz substrate measured at room temperature after annealing at different temperatures.

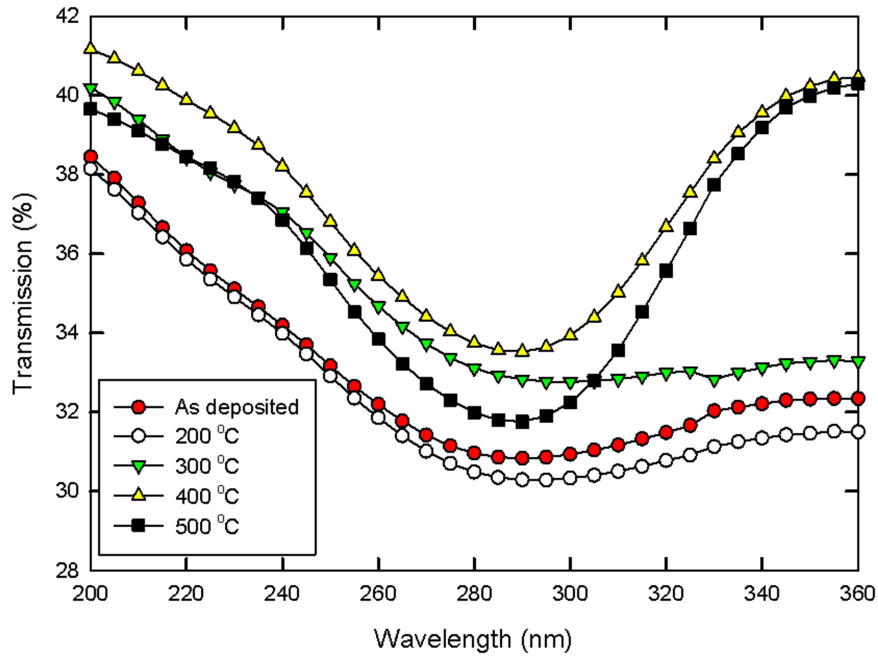

Fig. 10 Transmission vs. wavelength of a Ni/Ir/Au metal layer deposited on a quartz substrate measured at room temperature after annealing at different temperatures.

5.4 CONCLUSION

The reverse bias characteristics of the Ni/Au Schottky photodiode improved with annealing temperature up to 400 °C after which they deteriorated. The reverse bias characteristics of the Ni/Ir/Au photodiode continued to improve up to 500 °C annealing temperature, probably due to the Ir layer acting as a diffusion barrier. The Ni/Au Schottky photodiode exhibited a greater Schottky barrier height than the Ni/Ir/Au photodiode after annealing at 500 °C, the values of the barrier heights were 1.26 and 1.10 eV respectively. The Ni/Au photodiode exhibited a better responsivity of 0.077 A/W as compared to that of the Ni/Ir/Au photodiode which had a value of 0.025 A/W. The higher responsivity of the Ni/Au Schottky photodiode is attributed to the thinner metal layer used to produce the device, leading to lower absorption in the Schottky contact. The photocurrent to reverse current ratios at low reverse voltages reached as high as 10^2 for illumination at 2.1×10^{-9} W/cm^2 at 275 nm. Annealing the Ni/Au metal layer up to 500 °C resulted in the improvement of the transmittance of the contact. For optimal transmission, the best annealing temperature of the Ni/Ir/Au metal layer was found to be 400 °C and that of the Ni/Au 500 °C.

REFERENCES

[1] N. Miura, T. Nanjo, M. Suita, T. Oishi, Y. Abe, T. Ozeki, H. Ishikawa, T. Egawa, and T. Jimbo, Solid State Electron. **48** (2004) 689.

[2] S.M. Sze, Physics of Semiconductor Devices, John Wiley and Sons, New York, 1981.

[3] J.K. Sheu, Y.K. Su, G.C. Chi, W.C. Chen, C.Y. Chen, C.N. Huang, J.M. Hong, Y.C. Yu, C.W. Wang, and E.K. Lin, J. Appl. Phys. **83** (6), (1998) 3172.

[4] C.Y. Lu, E.Y. Chang, J.C. Huang, C.T. Chang, M.H. Lin, and C.T. Lee, J. Electron. Mater. **37**, (2008) 624.

[5] E. Monroy, F. Calle, J.L. Pau, J. Sanchez, E. Muñoz, F. Omnes, B. Beaumont, and P. Gibart, J. Appl. Phys. **88** (4), (2000) 2081.

CHAPTER 6

CONCLUSIONS

AlGaN based Schottky photodiodes have been successfully fabricated and characterised. The diodes were subjected to increasing annealing temperatures in order to investigate the evolution of their electrical and optical characteristics. The annealing was done in an Ar ambient since it is an inert gas. There was a dependence of the electrical properties on annealing. The Schottky photodiodes exhibited good thermal stability even after annealing at high temperatures. At temperatures higher than 400 ^{o}C the Ni/Au Schottky photodiode began to show signs of deterioration. The Ni/Ir/Au Schottky photodiode only began to degenerate after 500 ^{o}C annealing.

As the annealing temperatures were increased the Schottky barrier height of the Ni (50 Å)/ Au (50 Å) Schottky photodiode increased to a value of as high as 1.46 eV for *I-V* characteristics. The reverse current was decreased from 2.07×10^{-9} A to the order of 10^{-13} A at -2 V reverse bias voltage. The *I-V* Schottky barrier height of the Ni (20 Å)/ Au (50 Å) Schottky photodiode increased to as high as 1.26 eV while that of the Ni (20 Å)/ Ir (30 Å)/ Au (50 Å) increased to 1.10 eV. Their reverse currents decreased from 3.95×10^{-11} A to 4.94×10^{-13} A and from 3.73×10^{-12} A to 1.12×10^{-13} A respectively. The dependence of the electrical properties on annealing was probably due to the interfacial interactions at the metal-semiconductor contact.

With regards to optical characteristics of the Ni/Au and Ni/Ir/Au Schottky photodiode, the responsivity and the quantum efficiency were the two main optical characteristics extracted from the photocurrent measurements. A responsivity value of as high as 0.077 A/W at 200 nm was obtained for the Ni/Au Schottky photodiode and that of Ni/Ir/Au Schottky photodiode was 0.025 A/W at 275 nm. The UV to visible rejection ratio was as high as 10^{3} for the Ni/Au Schottky photodiode and 10^{2} for the Ni/Ir/Au Schottky photodiode.

For the metal layers on the quartz substrate, the transmittance was dependent on the type of metal deposited and on the metal layer thickness. As expected, the transparency of the Ni/Au

metal layers was higher than that of the Ni/Ir/Au layers, which included an additional Ir layer. As the metal layers were annealed the transparency of the metals to UV light increased depending on the metal layers, spectrum of radiation and annealing temperature. The transmittance of the Ni (50 Å)/ Au (50 Å) metal layer increased from 43 % as deposited to 68 % after annealing at 500 ^{o}C in the wavelength range 200 to 350 nm. The transmittance of the Ni (20 Å)/ Au (50 Å) metal layer increased from 57 % as deposited to 84 % after annealing at 500 ^{o}C in the 200 to 360 nm wavelength range. The transmittance of the Ni (20 Å)/ Ir (30 Å) / Au (50 Å) layer, however, showed a different pattern to the Ni/Au metal layers. It decreased from as deposited to 200 ^{o}C and then increased with annealing temperature up to 400 ^{o}C and then again decreased after 500 ^{o}C annealing. The transmittance measured at these different temperatures varied between 30 % and 41 % in the 200 to 360 nm wavelength range. This is ascribed to the Ir interacting with the Ni and the Au as this behaviour was not evident in the Ni/Au metal layers. The transmittance was also dependent on the wavelength of the radiation.

Further Studies:

Further work has to be done in order to look at how to improve both the optical and electrical characteristics of Schottky photodiode. Defects play a significant role in determining the characteristics of Schottky diodes. The presence and properties of defects may be investigated by means of Deep Level Transient Spectroscopy (DLTS). The reverse I-V characteristics of these diodes indicate that some defects may be present therefore this might be a fruitful study. Furthermore, these devices may be used in radiation environments (e.g. space) where defects may be induced by energetic particles. This can be simulated in the laboratory by bombarding the semiconductor with ions in order to create defects and investigate whether these have an enhancing or degenerating effect on a fabricated device. The defects in the AlGaN material can affect the current including the photo generated current of the photodiodes. Since these defects might also react during annealing, a DLTS study coupled to an annealing study might yield interesting results.

Also, further annealing studies can be investigated for different ambient conditions, for instance using different gases. Varying the thicknesses of the metals and using different metals and metal combinations can also help to optimise the metal layers and thus improve the Schottky photodiode.

Correlation between electrical properties and chemical changes in the contacts could be investigated by means of X-rays Photoelectron Spectroscopy (XPS) and Auger Electron Spectroscopy.